The cellular landscape of the endochondral bone highlights its multipotent and immunomodulatory features during the transition to extrauterine life.

Alejandro Díaz Rueda[1,4], Irepan Salvador-Martínez[2,4], Ismael Sospedra-Arrufat[1], Ana Alcaina-Caro[1], Ana Fernández-Miñán[1], Ana M. Burgos-Ruiz[1], Ildefonso Cases[1], Alberto Mohedano[3], Juan J. Tena[1], Holger Heyn[2], Javier Lopez-Rios[1,*], and Gretel Nusspaumer[1,*]

[1]Centro Andaluz de Biología del Desarrollo (CABD), CSIC-Universidad Pablo de Olavide-Junta de Andalucía, 41013 Seville, Spain.

[2]CNAG-CRG, Centre for Genomic Regulation (CRG), Barcelona Institute of Science and Technology (BIST), 08028 Barcelona, Spain.

[3]Intensive Care Unit, Severo Ochoa University Hospital Leganés, 28911 Madrid, Spain.

[4]These authors contributed equally

*Correspondence: jloprio@upo.es, gnusda@upo.es

Abstract

The cellular complexity of the endochondral bone underlies its essential and pleiotropic roles during organismal life. While the adult bone has received significant attention, we still lack a deep understanding of the perinatal bone cellulome. Here, we have profiled the full composition of the murine endochondral bone at the single-cell level during the transition from fetal to newborn life and in comparison to the adult organ, with particular emphasis on the mesenchymal compartment. The perinatal bone contains different fibroblastic clusters with blastema-like characteristics in organizing and supporting skeletogenesis, angiogenesis, and hematopoiesis. Our data also points out to a dynamic inter- and intra-compartment interactions as well as a bone marrow milieu prone to anti-inflammation, which we hypothesize is necessary to ensure the proper program of lymphopoiesis and the establishment of central and peripheral tolerance in early life. Our study provides a integrative roadmap for the future design of genetic and cellular functional assays to validate cellular interactions and lineage relationships within the perinatal bone.

INTRODUCTION

Important changes take place during the transition from intrauterine to extrauterine life. The newborn is reaved of nutrients, heat and the buoyant and pathogen-protected environment of the womb. Among other large organismal changes, lungs are inflated and the cardiovascular flow adjusted as the newborn starts breathing. High hormonal levels are present in preparation for the sharp increase in the metabolic rate and thermoregulation. Brown fat tissue, accumulated during late gestation, plays an important metabolic and thermal role during the first days of life. Increased mechanical load and movement impacts on the skeleton of the newborn, where the osteogenic program will also be affected by the increase in oxygen supply. The establishment of the intestinal microbiome and its crosstalk with the still immature immune system will impact as well on the program of hematopoiesis in the bone marrow which started to build at late fetal stages[1-4]. The skeleton has a pivotal position in many of these processes, given its roles in body support, movement, organ protection, hematopoiesis and hormonal and metabolic control.

Endochondral bone-derived mesenchymal progenitors are able to engage in chondrogenic, osteogenic and adipogenic programs of differentiation, in addition to their specialization into bone marrow stromal cells (BMSC) that support hematopoiesis[5]. Development of long bones is a dynamic and tightly orchestrated process which reflects the capacity of mesenchymal progenitors to first generate cartilage, which will serve as a mold and will provide the signals to start the program of osteogenesis and the formation of the bone marrow (BM)[6-8]. During the formation of the BM, some mesenchymal progenitors will stay as BMSC, supporting hematopoiesis, but will also hold the capacity to differentiate into osteoblasts and adipocytes[9-11]. Genetic cell-fate tracking, prospective immunophenotype characterization and, recently, scRNAseq studies in the mouse are revealing the complex nature of the bone mesenchymal compartment, as well as the versatility of the different populations and their division of labor[12]. For example, the capacity of hypertrophic chondrocytes to transdifferentiate into osteoblasts is now well accepted in the field[13-15]. Moreover, bone fracture and fingertip regeneration mouse models,

along with studies on limb regeneration in other vertebrates, are challenging ingrained concepts and pointing to alternative models by which different populations (e.g. fibroblastic populations) can be recruited and reprogrammed in a highly plastic fashion, which includes cellular phenotypic convergence[10,13,16-20]. Most of these studies have nevertheless focused on the adult bone, and we still lack fundamental knowledge on the heterogeneity, relations and interactions between the mesenchymal and hematopoietic compartments at perinatal stages. To capture the main key features of these processes, we have generated a comprehensive scRNA-seq cellular map of all mouse endochondral bone compartments just before and after birth (E18.5 and postnatal day [PN] 1). The analysis of these datasets, in comparison with those from adult mice[21], uncovers that the composition and molecular fingerprint of several bone populations change significantly between these stages. Of note, our study reveals the presence of distinct perinatal fibroblastic mesenchymal populations with molecular signatures involving them in the formation of the bone marrow, organization of angiogenesis and peripheral innervation, as well as in the establishment of the environment for proper hematopoiesis, including putative direct interactions between specific mesenchymal and hematopoietic clusters. Notably, our study identifies some mesenchymal clusters with active immunomodulatory transcriptional programs which may be involved in setting an anti-inflammatory setup with implications for the maturation of the immune system and the self from non-self discrimination that is just starting to take shape. Overall, our findings highlight the relevance of integrative ontogenic studies that take into account the full cellular complexity of the endochondral bone and have important implications for the prospective isolation of cell populations for tissue engineering applications as well as for the age-tailoring of disease treatments.

RESULTS

A cell atlas of the perinatal endochondral bone

To get a comprehensive understanding of the composition, dynamics and roles of the endochondral bone in the transition from intrauterine to extrauterine life, with particular emphasis on the mesenchymal compartment, we adopted a FACS-enrichment

strategy that ensured that all cellular components of the E18.5 and PN1 endochondral bone could be captured by scRNA-seq in a balanced manner. This strategy is similar to that previously employed for adult bone[21], and allows to investigate not only the relationships between mesenchymal subpopulations, but also their involvement in angiogenesis, hematopoiesis, and peripheral nervous system development. To represent both abundant and minor populations, we employed the sorting strategy depicted in Fig. 1a (see also Materials and Methods). Briefly, dead cells and multiplets were excluded by gating, and no lineage labeling was used to prevent the loss of any cell subsets. The gates were defined by the use of a mix of pan-antibodies to mesenchymal (CD140a/PDGFR-a) and endothelial cells (CD31/PECAM), together with CD9, a marker highly expressed in early hematopoietic progenitors and stromal cells (nicheview.shiny.embl.de[21]). Sorted cells were mixed in different proportions to over-represent less abundant populations (Fig. 1a). While this strategy is not quantitative, it allows monitoring relative changes in cell number between equivalent clusters at both stages. After QC, 7,272 (E18.5) and 7,277 (PN1) high-quality cells were recovered for analysis, with a mean of 2,625 and 2,533 genes per cell, respectively.

A combination of unsupervised and curated clustering led to the annotation of 24 cell populations, each displaying a distinct molecular signature (Fig. 1b, c, Fig. S1 and Fig. S2). These clusters encompass all hematopoietic, mesenchymal and endothelial compartments in the perinatal endochondral bone. The entire hematopoietic compartment (HC, encircled in dark blue) and each of its clusters are characterized by the expression of defining markers such as *Ptprc* (pan-HC), *Cd79a* (B-Lin), *CD200r3* (Eo-Bas), etc. Recent scRNAseq, scATAC and scProteo-genomic data have demonstrated that FACS-isolated oligopotent progenitors represent heterogeneous mixtures of progenitor populations[22-24]. Not being our primary focus, we opted for broad categories for the definition of HC clusters. For instance, HPC (hematopoietic progenitor cells) encompasses granulocyte/monocyte progenitors, megakaryocyte progenitors and LMPP (Lymphoid Myeloid Primed Progenitors); likewise the B-Lin cluster includes all stages of B cell maturation. The endothelial compartment consists

of a single cluster (EC; encircled in purple in Fig. 1b), defined by the expression of pan-endothelial genes as *Cdh5 or Pecam1*/CD31.

Within the mesenchymal compartment (MC; encircled in light green), clusters corresponding to fate-committed progenitors or to differentiated cells were readily identified according to their molecular signature (Fig. 1b, c, Fig. S1 and Fig. S2). The chondrogenic (ChC) cluster was defined by the expression of the *Sox9*/*Sox5*/*Sox6* trio, which drives the transcription of *Col2a1, Acan, Col9a1, Col9a2* and *Col9a3* (ref. 25). The osteogenic (OsC) cluster was labelled by the expression of *Runx2*, *Osterix*/Sp7, *Bglap*/Osteocalcin, *Spp1*/Osteonectin and *Isbp*/bone sialoprotein[26]. Finally, the myofibroblast (Myo) cluster was characterized by the expression of key myogenic genes such as *Pax7*, *Myf5, Msc, Myod1* and *Acta2/aSMA*[27]. In addition, we defined seven closely-associated clusters of fibroblastic nature. These included a cell population with tenogenic characteristics (TC)[28-32], expressing *Scx*/Scleraxis, *Tnmd*/Tenomodulin, *Kera/*Keratocan and Cpxm2, and an articular cartilage progenitor (ACP) cluster expressing *Sox5*, *Gdf5, Pthlh*, *Barx1*, *Prg4, Wnt4* (Fig. 1c, Fig. S1 and Fig. S2)[33,34]. We also identified *Tspan15* and *Ackr2* as novel ACP markers, with implications in bone growth and remodeling[35-37]. The remaining five mesenchymal clusters were even closer in the UMAP space and annotated as GFP (*Gas6*$^{+}$ Fibroblastic Population, also enriched in *Eln*-expressing cells), SFP (Sca-1*/Ly6a*$^{+}$ Fibroblastic Population, expressing other markers such as *Ly6c1*), AFP (Adipogenic Fibroblastic Population, expressing *Ptch2* and *Notch3*), CLFP (*Cxcl12*-Low Fibroblastic Population, expressing *Ly6h* and *Lpl*) and PFP (Proliferating Fibroblastic Population) (Fig. 1c, Fig. S1 and Fig. S2). The PFP population is composed of cells in S or G2/M phases of the cell cycle and expresses mitogenic genes such as *Mki67, Nusap1, Cenpe* and *Ccna2* (Fig. 1c, Fig. S1 and Fig. S2). PFP contains the proliferating fractions of the GFP, SFP, AFP and CLFP clusters, but minimally of ACP, which fits the long-lasting quiescency of articular progenitors[38]. Cell-cycle analysis also revealed small proliferating subsets within other hematopoietic and mesenchymal clusters, including ChC and Myo (Fig. S2b, c). The comparison of cluster ratios showed significant changes in both hematopoietic and mesenchymal compartments accompanying the transition to extrauterine life, including a marked increase in the

representation of SFP, AFP and TC clusters at PN1 when compared to E18.5 (Fig. 1d).

Highlighting the differences between perinatal and adult bone mesenchymal compartments

Next, we used Harmony[39,40] to integrate our perinatal scRNA-seq datasets with those previously reported for adult[21] (Fig. 2, Fig. S3 and Fig. S4). This analysis indicated a good broad correlation between both stages, with related clusters falling into equivalent positions within the integrated UMAP space, with the exception of PFP, which was disconnected from the main fibroblastic clusters and split into three components (asterisks in Fig. 2a). Cell cycle analysis showed that, in contrast to perinatal stages where all compartments are proliferating, only the adult hematopoietic compartment displays cells in S and G2/M phases (Fig. 2b). Focusing on the mesenchymal compartment, adult chondrocytes and myofibroblasts had perinatal counterparts. The closely associated SFP, GFP, AFP and CLFP perinatal clusters localized in similar UMAP coordinates as the adult endosteal, arteriolar and stromal fibroblasts, while perinatal ACP and TC were not clearly identified in the adult scRNAseq dataset (see Discussion).

One of the most studied bone mesenchymal populations are CARs (*Cxcl12*-abundant reticular cells[41]). Seminal studies in the last decade have identified their pivotal role in hematopoiesis[42]. Adult CARs are also characterized by the expression of *Kitl* and represent almost all LepR+ cells (Fig. 2c)[43,44]. scRNAseq studies have further subdivided CARs in view of their adipogenic (Cxcl12+, Alpl-) or osteogenic profiles (Cxcl12+, Alpl+)[21,45] and even in more subsets[46-48], reflecting their adipogenic, osteogenic and BMSC differentiation potential. The comparison between equivalent UMAP plot coordinates at perinatal and adult stages (boxed area in Fig. 2c) revealed the almost complete absence of AdipoCARs in the perinatal bone and markers highly detected in adult Adipo-CARs (*Lepr, Cxcl12, Kitl, Pparg, Adipoq and Vcam1/*CD106)[10,49] were expressed in very few cells at perinatal stages, next to the OsC cluster (Fig. 2c). These results suggest that Adipo-CARs are just arising at perinatal stages and are in keeping with other reports using LepR antibodies, *Lepr-*

CreER lines induced in the early postnatal life and recent scRNAseq analysis of the stromal compartment at postnatal day four[11,50,51]. Of note, *Cxcl12, Kitl, Gas6* and *Lpl* were all expressed at lower levels in fibroblastic clusters, mainly in CLFP, AFP and GFP (Fig. 2c and Fig. S3), opening the possibility that some of the Adipo-CAR progenitors are contained within these clusters. In line with this possibility, also *Pparg* and *LepR*, important players of the adipogenic program that starts to shape perinatally, are expressed in a scattered manner in the perinatal fibroblastic clusters, including AFP cells (Fig. 2c and Fig. S3). In contrast, there is a good correlation between the perinatal OsC cluster and the adult osteogenic cells, which include Osteo-CARs and osteoblasts, with high expression of osteogenic genes (Fig. 2c and Fig. S3). As others have described for adult bone[21,52,53], we also located the perinatal prospective mSSC (murine Skeletal Stem Cells[54], characterized by the immunophenotype CD51+ CD200+; negative for CD45, CD31 and TER119, CD90, CD105, 6C3; Fig. S4a) in the osteogenic-related OsC cluster. The integral analysis of all endochondral cell populations (ref. 21 and this study) also reveals, with high resolution, the spatial and temporal (perinatal versus adult) expression patterns of reported genetic drivers and surface markers, providing an important resource for the interpretation of previous observations using cell-fate tracing mouse models and prospective isolation strategies (Fig. S4). A key advantage of including all bone endochondral populations in scRNA-seq experiments is that it provides a rich resource for the identification of markers restricted to specific populations. To illustrate this point, we identified different genes with preferential expression in the different perinatal fibroblastic clusters, which will allow the design of more precise inducible genetic tools (Fig. S5). Stressing the relevance of performing ontogenic studies, we identified genes active at perinatal stages that are not expressed in the adult tissue.

Hierarchical relations in the mesenchymal compartment

Next, we generated a new Harmony representation of only the mesenchymal clusters to better illustrate their relations at E18.5 and PN1 (Fig. 3a). As previously mentioned, we observed an increase in SFP and TC populations after birth. In the case of TC (labeled by *Scx* and *Tnmd*), two different branches can be detected. One of these is related to the chondrogenic cluster, while the other branch likely represents tenogenic

precursors as is preferentially labelled by additional tendon markers such as *Mkx* and *Kera* (Fig. 3b). In addition, we identified *Ptx4* as a novel tenogenic-specific gene, making it a good candidate for designing genetic tools to study tendon development/regeneration.

In order to identify potential hierarchical relationships within the mesenchymal compartment, we utilized PHATE (Potential of Heat-diffusion for Affinity-based Trajectory Embedding)[55]. In contrast to other tools, PHATE works in an unbiased manner without imposing assumptions on the structure of the data. Since PFP represents the proliferative fraction of GFP, SFP, TC and CLFP, we excluded it from this analysis. PHATE placed fibroblastic populations (GFP, SFP, TC) at the base of a goblet-shaped projection, with more committed clusters (OsC, Myo and ChC and pChC) projecting away from it (Fig. 3c). SC and Myo appeared as disconnected populations. The AFP population branches out but remains adjacent to GFP, CLFP is connected to SFP and GFP, and ACP forms a continuum with SFP (Fig. 3c and Supplementary Video 1). Gene Ontology (GO) analyses of GFP, SFP, AFP and CLFP at E18.5 and PN1 further revealed the nature and putative roles of these clusters (Fig. S6). These results associated CLFP, GFP and SFP to extracellular matrix (ECM) organization and angiogenesis. AFP GO terms link it with the regulation of osteoblast and fat differentiation, as well as with brown fat cell differentiation and cold-induced thermogenesis, the latter term also shared by CLFP and GFP. Fat metabolism is essential in the first hours postpartum, in preparation for starvation and thermoregulation[2,56]. AFP GO terms also associate it to myeloid and B cell differentiation, branching morphogenesis -a key feature of vessel formation, and glial cell differentiation. SFP GO terms are related to cell migration and cell adhesion, regulation of nitric oxide synthesis, leukocyte differentiation, coagulation and wound healing. GFP displays GO terms for ossification, osteoblast differentiation, response to mechanical stimulus, fibroblast proliferation, cartilage development, hormonal regulation and glucose homeostasis[3]. CLFP is also associated to bone mineralization, ossification, glial cell migration (along with SFP), regulation of muscle cell differentiation and axon guidance. This plethora of putative tasks support a pivotal role for perinatal fibroblastic clusters in the bone under construction and in the transition to

postnatal life. In support for these broad organizing functions, we noted that the perinatal fibroblastic cluster signatures include genes previously identified in the blastema that forms after digit tip amputation in adult mice, including *Mest1*, *Ltbp2*, *Scara5*, *Clec3b* and *Cd34*, the latter three expressed in dermal-derived fibroblasts (Fig. 3d and Fig. S4)[16,17].

Interactions between endochondral cell subsets and implications for central tolerance

To gain insight into the interconnectivity of the different perinatal bone cell populations, we used CellPhoneDB, an algorithm based on the expression pattern of ligands, receptors and ECM components, therefore capturing both direct and indirect interactions[57]. The degree of interaction within mesenchymal clusters (MC-MC) and between MC clusters and EC (MC-EC) or hematopoietic clusters (MC-HC) is shown in Fig. 4a. In all three compartments, cluster interactions were higher at E18.5 than at PN1. MC-MC displayed the highest number of calls, being TC, OsC, SFP and GFP the most interacting clusters, and Myo the least. ECM components such as collagens and integrins were the most abundant connectors, as expected for fibroblastic populations, with several stage-specific differences (Tables S1-S3). The type of collagens and integrin complexes was highly diverse and different clusters displayed specific profiles (Table S3), which fits the dynamic properties of the matrisome, which changes according to age and inflammatory conditions[58]. For example, a significant difference between E18.5 and PN1 was the lack of integrin a1b1 complex at PN1 in GFP, ACP and OsC clusters. This integrin complex is associated with remodeling and wound healing[59]. Membrane-bound COL13A1, relevant for bone growth, was mainly expressed by OsC and EC clusters[60,61]. This analysis also identified the interconnection of SC with several other subsets through *Col20a1* and a1b1/a2b1 integrin complexes. *Col20a1* is SC-specific and expressed only at perinatal stages (Fig. S1, Fig. S2 and nicheview.shiny.embl.de[21]). As the ECM participates in signaling, migration, lineage specification and compartmentalization in several tissues[62], these changes might dictate a code involved in the spatial and temporal organization of the skeletal program[63].

Next, we explored direct interactions (no secreted molecules, p-value <0.05, Log2 mean > -1; Table S4 and Table S5), and focused on those clusters displaying the highest number of partners and the strongest connectors. Within the MC, the SFP and OsC clusters appeared as the most dynamic (Fig. 4b), with CADM1 and COL13a1 mediating significant interactions in the latter. NOTCH and their ligands were highly prominent among fibroblastic clusters, as expected from their important roles in bone development and homeostasis[64]. DLK1-NOTCH1 and DLK1-NOTCH2 mediated very strong connectors in all mesenchymal clusters and with EC (not indicated in Fig. 4b to allow the visualization of other interactions, see Table S1-S5). DLK1 is a non-canonical ligand that inhibits NOTCH1 receptor activity[65]. Of note, *Dlk1* is not expressed in adult bone (nicheview.shiny.embl.de[21]), whereas at perinatal stages it is restricted and highly expressed in most of the clusters of the mesenchymal compartment. NOTCH3 mediated various connectors, mainly in AFP, which is relevant as *NOTCH3* mutations cause Lateral Meningocele Syndrome (OMIM #130720), characterized by several skeletal abnormalities[64]. In addition, the highly prevalent JAG1-NOTCH3 pair could play a role in vasculature remodeling, as slow-cycling LepR:Cre *Notch3*+ cells were closely associated to vasculature in the bone marrow of adult mice[48]. In fact, EC displayed a high number of direct interactions with GFP, OsC, AFP, CLFP and Myo, mainly through selectins (SELL, SELP, SELE), supporting our previous GO analyses that associated AFP and CLFP with different aspects of angiogenesis (Fig. 4b and Fig. S6). Schwann cells (SC) also showed broad direct interactions with SFP, AFP, OsC, CLFP and with themselves (Table S4). In particular, we identified a specific link mediated by CADM3 (exclusive of SFP) and CADM4 (exclusive of SC) (Fig. 4c). Future studies will determine the relevance of this interaction, but CADM3 mutations are associated to type 2FF Charcot-Marie-Tooth disease (OMIM #619519), a peripheral neuropathy with early childhood onset and characterized by progressive weakness and muscle atrophy[66]. In this context, both *Col20a1* and *Cadm4* are excellent candidate *loci* for the design of genetic tools to address peripheral nervous system regulation of endochondral bone development and regeneration[67].

Concerning the hematopoietic compartment, several of the MC clusters interacted with HPC, and preferentially with Eo/Bas and ILC-TSP2 being GFP, SFP, AFP and CLFP the most active (Fig. 4a). Representative direct connectors for HPC, ILC-TSP2 and Eo/Bas are APP-CD74, ICAM1-ITGAL and SELL-CD34, respectively (Fig. 4b and Table S5). While adult/perinatal Eo/Bas and B lineage cells map to equivalent coordinates in the UMAP space, there are significant differences between perinatal ILC-TSP2 cells and adult NK and T cells (Fig. 4d and Fig. S7). T cells in the adult bone marrow correspond to memory T cells and regulatory T cells[68]. The T cell cluster in the adult scRNA-seq dataset (nicheview.shiny.embl.de[21]) highly expresses all CD3 components of the TCR receptor (*Cd3e*, *Cd3g*, *Cd3d* and *CD247*/TCR zeta) in addition to CD8a and CD8b1, identifying them mostly as memory CD8 T cells. In contrast, perinatal ICL-TSP2 cells only transcribe *Cd3g* and *CD247*, do not express *Lef1*[69] and are negative for *Sell*/CD62L and *Ccr7* genes expressed in central memory T cells[70]. In line with recent scRNAseq data on thymus seeding progenitors[71] (TSP), we named this cluster ILC-TSP2 on the basis of the expression of *Cd7, Itgb7, Irf8, CD3e (CD3g* in mouse) and the absence of *Hoxa9* and *Cd34* transcripts[72,73]. Of note, we identified ILC-TSP2 as the only cluster expressing *Ccl5* (Fig. S1 and Fig. S7). This is relevant because callus formation in bone fracture models depend on the expression of the Ccl5 receptors Ccr5 and Ccr3 in periosteal Mx1+Acta2/aSMA+ cells[74], which highlights the relevance of the crosstalk between the MC and HC (see also additional ILC-TSP2 markers[75,76] in Fig. S1). The role of the Eo/Bas cluster at these stages is less characterized. Perinatal Eo/Bas specifically expressed high levels of anti-inflammatory interleukins *Il4* and *Il13* (Fig. S1 and Fig. S7). In keeping with an anti-inflammatory setup, we also observed the lack of expression of MHCII genes (*H2-Aa* and *H2-Eb1*) in monocyte and dendritic cells (Mon DC), and a high expression of *Il1rn* and *Il1r2* (both encoding decoy receptors of pro-inflammatory IL1) in monocytes and neutrophil clusters. In addition, monocyte, neutrophil and Eo/Bas clusters express high levels of *Osm* (Oncostatin M), which stimulates osteogenesis and inhibits adipogenesis[12], further highlighting the interdependency of the different cellular components (Fig. S7).

Main transcriptional networks and immunomodulatory properties of the mesenchymal compartment within the perinatal endochondral bone

To shed light on the transcriptional programs operating in the mesenchymal compartment, with special emphasis on the fibroblastic clusters, we utilized SCENIC (Single-Cell rEgulatory Network Inference and Clustering)[77,78]. This tool can detect the activation of gene regulatory networks controlled by a given transcription factor [called "regulons", noted with a (+) symbol] based on the expression of its cognate targets, even if the upstream TF was not captured in the scRNA-seq data. Conversely, SCENIC labels regulons as not active if not sufficient targets are expressed, even if the controlling TF is detected. The top-ten regulons at E18.5 and PN1 and the differentially active intrauterine and extrauterine regulons are shown in Fig. S8. SCENIC accurately captured biologically relevant regulons in chondrogenic [Sox9(+), Sox5(+); ChC and ACP], osteogenic [Runx2(+), Sp7(+), Dlx5(+); OsC] and adipogenic [Pparg(+), Gata6(+), Prdm6(+); AFP and GFP] clusters (Fig. S9). Concerning the latter differentiation program, *Pparg* is a key adipogenic regulator, while *Gata6* has been recently associated to brown adipogenesis[79], in agreement with our GO analysis. Finally, GWAS studies have linked *PRDM6* to obesity and osteoporosis[80], and another family member, *Prdm16*, has been implicated in brown fat differentiation in early myoblast progenitors[81,82]. The CLFP population shared several active regulons with the Myo cluster [MyoG (+), Msc(+), Myf5 (+) and MyoD (+)], suggesting that these two populations could be related. Mkx(+) was the most-significant regulon in TC (Fig. 3)[83,84]. Two additional key observations could be extracted from the SCENIC analysis. Firstly, several Hox regulons were active in GFP, SFP, TC and ACP clusters (Fig. S8). While *Hox* functions have been most studied in the context of axial and limb patterning[85], it has been described that periosteal Hox+ fibroblastic populations contribute to bone repair in adult fracture models[86]. Secondly, several of the most prominent regulons in SFP and ACP were related with inflammation and showed multiple cross-regulatory interactions (tables in Fig. 5). *Nfkb1*, one of the most prominent regulons detected by SCENIC, encodes p105 and its processed form p50. Dimers of p65 (the class 2 subunit of NF-κB transcription factor, encoded by *RelA*) and p50 trigger a pro-inflammatory response. The NF-κB pathway is negatively controlled by p50/p50 homodimers that outcompete p65/p50 dimers and also

suppress pro-inflammatory gene expression by association with other proteins like HDACs and p300[87]. p50/50 homodimers can also promote the expression of anti-inflammatory genes by association with Bcl3[88], and the Bcl3(+) regulon itself is active at E18.5 and PN1 and controls *Nfkb1* expression (Fig. 5 and Fig. S8). Another active regulon involved in inflammation regulation and active at E18 and PN1 is Atf3(+)[89]. ATF3 has been shown to inhibit NF-κB pathway by dimerization with p65 and recruiting HDAC1[90]. *Klf3* is a transcriptional repressor that directly suppress the expression of *RelA*[91], and its regulon is active only at E18.5. Of note, the Klf4(+) regulon is detected as active at PN1. In addition to its role in osteogenesis[92], *Klf4* participates in several cellular processes depending on the cellular type and context[93] and it can act as either a pro- or anti-inflammatory factor[94-97]. The Cebpd(+) regulon modulates different cellular processes[98], and is mainly related with inflammatory response in macrophages but can also act in preventing deleterious effects of the inflammatory response[99,100]. Other regulon active only at PN1 and associated with inflammatory regulation is Nr1d1(+) (Nr1d1/Rev-Erbα encodes a core protein of the circadian clock)[101-103]. Interestingly, and still not explored in depth, different *Hox* genes interact with the NF-κB pathway and intervene in different aspects of inflammation[104,105].

Strategies for the prospective isolation of mesenchymal populations

Based on their molecular profiles, the well-characterized PαS population [immunophenotype: Lineage negative (CD45, TER119, CD31) and PDGFR-a+, Sca-1+] corresponds to the SFP, ACP and part of the GFP clusters. PαS were first described in adult bone[106] and these Sca-1+ (encoded by *Ly6a*) fibroblastic populations have been shown to contain multipotent progenitors able to give rise to cartilage, bone and adipose tissue[106-109]. In addition, Sca1+ cells in the periosteum highly contributed to the formation of the callus in fracture models[10,48,53,110,111]. PαS are most abundant at perinatal stages, but less represented in adults, where they are restricted to the compact bone[106,107,112]. These properties, together with the immunomodulatory profile of SFP and ACP revealed by the SCENIC analysis, make PαS an important target for biomedical applications. Hence, developing robust isolation strategies is key for the isolation of the human equivalent populations for use

in cellular therapies, but as there is no human ortholog of the *Ly6a*/Sca-1 gene[113], additional reliable markers need to be identified. To do so, we interrogated our scRNA-seq datasets for several surface markers that were evolutionary conserved between mouse and human and validated them by FC in order to develop an alternative isolation strategy to enrich in PαS cells without resorting to the use of Sca-1 antibodies. The final strategy and best markers assayed to enrich in SFP, ACP and CLFP populations are shown in Fig. 6. All lineage negative *Ly6a*/Sca-1+ cells were PDGFR-α+ (Pa+), *Pdpn*/gp38+, *Cd55*+ and mostly *Entpd1*/CD39 negative (Fig. 6b). CD39+ Pa+ defined the CLFP population, while CD55 was highly expressed in ACP and SFP, with *Thy1*/CD90 only labeling SFP (Fig. 6a and 6b). These profiles allowed devising a strategy to purify CLFP, SFP and ACP populations in three steps (Fig. 6c). The separation between SFP (CD90+) and ACP ($CD90^{neg}$) within $CD55^{hi}$ cells was confirmed using Sca-1 and CD90 staining. While this strategy is suitable for perinatal stages, *Entpd1*/CD39 is not expressed in adult populations (nicheview.shiny.embl.de), which illustrates the importance of performing ontogenic studies and adapt the prospective immunophenotype to the specific stage under analysis.

DISCUSSION

As previous scRNAseq studies have shown, the adult bone mesenchymal compartment is very diverse and our study uncovers how such complexity starts to build up in early life. Our analysis reveals different clusters of fibroblastic progenitors at perinatal stages, with diverse potentials as indicated by GO, cell trajectory and gene regulatory network tools. These analyses unveiled that the most uncommitted clusters (GFP, SFP, AFP and CLFP), in addition to their potential to regulate osteogenesis, adipogenesis and chondrogenesis, are also involved in a wide spectrum of tissue-organizing functions, including the regulation of hematopoiesis, angiogenesis, innervation, extracellular matrix organization, metabolism and hemostasis. For instance, AFP representation increased after birth and, along with the GFP population, is associated to adipogenesis, including brown fat differentiation and cold-induced thermogenesis, so important to control caloric restriction and temperature once the protection of the placenta is lost[2]. LepR+ CAR cells, highly represented in adults[114],

were not present at perinatal stages. This is not due to the enrichment strategy used, since this population was barely detected by FC from total bone enzymatic cell suspensions using the CD106/Vcam1 Adipo-CARs marker (data not shown). Our findings are in line other studies, the most recent one by the Morrison group[51], which shows that Adipo-CARs are just emerging at postnatal day 4. Interestingly, AFP could represent a precursor of Adipo-CARs, since it was the main and almost exclusive cluster expressing *Notch3*. *Notch3*-expressing cells targeted by LepRCre in adults showed to be multipotential slow cycling cells[48]. Two other clusters that were more prominent after birth were SFP and TC. While the absence of an equivalent TC cluster in adults could be related to differences in sample preparation methods, both TC and several of the fibroblastic progenitor clusters displayed differential molecular fingerprints previously identified as specific of the blastema during digit tip regeneration in adult mice (e.g. *Mest* expression). These results fit the previous observation that digit tip blastema cells are more similar to bone-derived mesenchymal cells at PN3 than to those of adult and largely differ from those of the limb bud[17]. In amphibian limb amputation models, successful regeneration requires the dedifferentiation of connective tissue and dermal fibroblasts in order to rebuild the skeleton[18]. Hence, the complex set of perinatal fibroblastic populations we have identified in this study -some of which also have dermal signatures- may act as reprogramming, specification and differentiation organizers of bone structure during these dynamic stages in which the bone marrow is under active construction to establish definitive hematopoiesis and during which osteo-chondrogenic programs are very active. The granularity of our study allowed the identification of various fibroblastic populations with distinct molecular identities and putative roles in these organizative processes, and our profiling of markers and active gene regulatory networks provides an entry point for the prospective isolation -as we show for SFP, ACP and CLFP- and *in vitro* expansion of some of these specific cell subsets for tissue engineering approaches. Besides, the identification of cluster-specific genes will allow the design of more precise inducible genetic mouse lines for cell fate tracking or cell population depletion. As the system reaches the steady state after sexual maturity, these fibroblastic populations become less abundant and get restricted to the compact bone in a slow-cycling self-renewal state with osteo-chondrogenic potential, while BMSC

(such as LepR+ CARs) become prominent[10,11,48,50,115]. Only if the balance is broken, as demonstrated by bone fracture models, periosteal cells (e.g. with the PαS immunophenotype) and probably nearby connective tissue cells[18] reactivate the endochondral bone program for callus formation[10,13,20,53,110,111].

Our integral approach to capture all endochondral bone cell populations also allowed us to predict intra- and inter-compartment interactions of all mesenchymal clusters. For instance, in this study we identified that *Cadm3*, the ortholog of the human gene mutated in Charcot-Marie-Tooth type 2FF peripheral neuropathy[66], is specifically expressed by the SFP population and mediates a putative direct interaction with Schwann cells via CADM4. These analyses also unveiled the complex MC-HC connectome, in particular the abundant interactions of fibroblastic SFP, AFP, CLFP and GFP populations with HPC, and quite outstandingly, with the ILC-TSP2 and Eo/Bas clusters. From the immune perspective, these ILC-TSP2 interactions might play a role in the protection/maturation of thymus seeding progenitors for the establishment of central tolerance in the thymus and the generation of the first thymic regulatory T cells[116,117]. This hypothesis is supported by the recent identification of two populations of mesenchymal cells essential for thymus development with prospective signatures similar to those of bone GFP and SFP clusters[118]. Concerning the Eo/Bas cluster, we observed a high and exclusive expression of anti-inflammatory cytokines *Il4* and *Il13*. In line with our results, basophil cells in newborns were shown to skew the differentiation of T cells towards Th2, which in newborns have an anti-inflammatory profile to protect intestinal microbiota and prevent tissue damage[119,120]. Highlighting the interdependency between compartments, both hematopoietic clusters also express key factors mediating bone healing (*Ccl5*[74] in ILC-TSP2) and osteogenesis-adipogenesis balance (*Osm*[12] in Eo/Bas). Future studies will be required to address the potential relevance of these bi-directional interactions at perinatal, puberty and adult stages.

Another important finding from our study is the identification of several immunomodulatory transcriptional programs operating in mesenchymal clusters (SFP, ACP and, to some extent, GFP) that seem to be skewed towards an anti-inflammatory

response. These observations fit the previous proposal that the 2-week juvenile mouse bone provides an anti-inflammatory environment (with low expression of MHCI molecules in stromal populations) that changes to pro-inflammatory after sexual maturation[58]. In support of this, several mesenchymal clusters highly express *Dlk1*, a ligand previously shown to inhibit Notch-dependent pro-inflammatory cytokine production by macrophages[65]. In contrast to adult populations, macrophages neither express MHCII genes (*H2E-b1* and *H2A-a*) nor their protein products (also assessed by FC; data not shown), while neutrophils display high expression of the IL-1 decoy receptors *Il1rn* and *Il1r2.* An attractive hypothesis stemming from our results is that an anti-inflammatory environment of the perinatal bone marrow could ensure the proper balance between myeloid and lymphoid HSC lineage choice. High pro-inflammatory conditions promote HSC division and skew their differentiation towards the myeloid lineage at the expense of lymphopoiesis, potentially leading to excessive proliferation and exhaustion of HSC[121]. In addition, and particularly in early life where individuals are first exposed to pathogens, primary immune organs (bone marrow and thymus) should be protected from infections and the deleterious effects of a highly pro-inflammatory milieu, to ensure the establishment of a proper self-tolerance.

Finally, our study reveals significant cellular and gene expression differences between neonatal and adult stages which implies that therapeutical interventions targeting endochondral bone populations or compartments must be adapted according to the age of the patient.

FIGURE LEGENDS

Fig. 1. A cell atlas of the perinatal endochondral bone

(**a**) Gating strategy for the processing of cell suspensions for scRNA-seq, obtained after enzymatic digestion of forelimb long bones at E18.5 and PN1 (see Materials and Methods for details). The number of sorted cells that were mixed for each gate is indicated by the color codes in the FC pseudocolor plots.

(**b**) Uniform Manifold Approximation and Projection (UMAP) of annotated clusters at E18.5 and PN1. Mesenchymal cells (MC) are encircled in green, hematopoietic cells (HC) in dark blue, endothelial cells (EC) in magenta and Schwann cells (SC) in turquoise. Neu: neutrophils; Ery: erythrocytes; Im Neu: immature neutrophils; HPC: hematopoietic progenitor cells; PHP: proliferating hematopoietic progenitors; ILC_TSP2: innate lymphoid cells and thymic seeding progenitors 2; Eo Bas: eosinophils and basophils; Sca1 HC: Sca-1^{+} hematopoietic cells; Mon DC: monocytes and dendritic cells; Oc: osteoclasts; B Lin: B-cell lineage; SC: Schwann cells; PFP: proliferating fibroblastic population; ACP: articular cartilage population; TC: tenogenic cells; SFP: Sca-1^{+} fibroblastic population; GFP: *Gas6*$^{+}$ fibroblastic population; AFP: adipose fibroblastic population; CLFP: *Cxcl12*-low fibroblastic population; ChC: chondrogenic cells; OsC: osteogenic cells; Myo: myofibroblasts.

(**c**) Dotplot of the representative genes across perinatal (E18.5 and PN1) clusters. Dot color and size indicate average expression levels and percentage of cells in a cluster expressing the selected gene, respectively.

(**d**) Stacked-bar charts indicating the proportions of cells assigned to each cluster at E18.5 and PN1.

Fig. 2. Differences between perinatal and adult endochondral bone.

(**a**) UMAP plot of Harmony-integrated adult[21] and perinatal scRNAseq datasets. Note that the integration with adult data changes the distribution of the clusters in comparison to Fig. 1 (e.g. PFP, indicated by asterisks). PChC: proliferating chondrogenic cells.

(**b**) Cell cycle analysis of the Harmony-integrated adult and perinatal scRNAseq datasets. Arrowheads and dotted lines indicate G2/M clusters that in adult correspond

to HC (*Ptprc*+ and *Spn*+) and that in perinatal stages is part of the PFP mesenchymal cluster (positive for *Pdgfra*+ and *Prrx1*+).

(**c**) Genes expressed in CARs in adult versus perinatal stages (upper panels). Lower left box: enlarged view to compare the coordinates of AdipoCARs in adult and their absence in perinatal stages. Lower right panel: magnification of CAR clusters and overlay of Adipo- and OsteoCARs markers in adult and perinatal stages.

Fig. 3. Hierarchy between mesenchymal clusters of the perinatal bone

(**a**) Harmony integration of mesenchymal clusters at E18.5 and PN1. The two branches of the TC cluster at PN1 are labeled by a dotted line.

(**b**) Expression of TC-specific genes at E18.5 and PN1. Enclosed in a red dotted line is *Ptx4*, exclusive of the tenogenic branch.

(**c**) Trajectory visualization of perinatal mesenchymal clusters using PHATE in 2D (left panel) and 3D captures (right panels).

(**d**) Expression in perinatal and adult bone of genes identified in dermal and blastema cells in the mouse digit tip regeneration model.

Fig. 4. Cell to cell communication in the perinatal endochondral bone

(**a**) Total number of connections (Nº of calls) identified by the CellPhoneDB algorithm within mesenchymal clusters (MC-MC), between mesenchymal clusters and EC (MC-EC) and mesenchymal and hematopoietic clusters (MC-HC).

(**b**) Chord diagrams of the clusters showing the highest number of direct interactions (non-secreted proteins). The most significant connectors pairs are shown.

(**c**) UMAP projection at E18.5 showing the exclusive expression of *Cadm3* and *Cadm4* in SFP and CS, respectively, identified as a direct interaction between these clusters.

(**d**) UMAP coordinates comparing Eo/Bas, NK-Tcells versus ILC-TSP2 and B-cell clusters in perinatal and adult bone. Striking differences are observed between NK-T cells versus ILC-TSP2 (enclosed in red dotted box and indicated by red arrows).

Fig. 5. Immunomodulatory properties of the perinatal bone mesenchymal compartment

(**a, b**) SCENIC analysis of the MC at E18.5 (a) and PN1 (b) displaying the main immunomodulatory regulons. UMAP projections of the mesenchymal clusters at E18.5 and PN1 are shown as a guide for cluster identification. The tables show the regulons that control the expression of key transcription factors involved in immunomodulation (*Klf3*, *Klf4*, *Nfkb1*, *Cebpd* and *Nr1d1*). Colored in red are their regulons to show their autoregulation and the network of cross regulation. Lower panels depict the joint activity of the regulons Atf3(+), Nfkb1(+) and Klf3(+) at E18.5 and Atf3(+), Nfkb1(+) and Klf4(+) at PN1. The individual expression of the corresponding genes is displayed to the right of each SCENIC projection.

Fig. 6. Prospective identification of ACP, SFP and CLFP clusters in newborns

(**a**) Expression of surface markers suitable for FC analysis at perinatal stages. PαS (PDGFRa+, Sca-1+) cells encompasses clusters SFP and ACP. In addition, *Ly6a*/Sca1 is expressed in EC and Sca1HC. *Cd55* mirrors well the expression of *Ly6a* in the mesenchymal clusters. Within mesenchymal clusters, *Entpd*/Cd39 mainly identifies CLFP, while *Thy1/*CD90 is restricted to SFP.

(**b**) FC analysis comparing the expression of Sca-1 with the other prospective markers (CD55, CD39 and CD90) in the mesenchymal compartment of newborns (Lin^{neg} PDGFR-a+/Pa+ and gp38/Pdpn+). Dead cells were excluded as 7-AAD positive. Lin= Lineage (TER119, CD45 and CD31).

(**c**) A 3-step strategy not relying on the use of Sca-1 to enrich in SFP, ACP and CLFP populations. SFP (Lin^{neg} $PDGFRa^{+}$ $gp38^{+}$ $CD39^{neg}$ $CD55^{+}$ $CD90^{+}$); ACP (Lin^{neg} $PDGFRa^{+}$ $gp38^{+}$ $CD39^{neg}$ $CD55^{+}$ $CD90^{neg}$); CLFP (Lin^{neg} $PDGFRa^{+}$ $gp38^{+}$ $CD39^{pos}$). Pseudocolor plots are representative of at least 3 independent experiments at PN1, each cell sample being extracted from to 3-4 littermates. Similar results were obtained with E18.5 samples (data not shown).

MATERIALS AND METHODS

Mice (*Mus musculus*)

Adult C57Bl/6J females and males were purchased from Envigo and housed under pathogen-free conditions according to Spanish and EU regulations. All animal experiments were designed according to the 3R principles. Animals were set in natural matings and vaginal plugs checked to time the collection of samples at E18.5 and postnatal day 1. Individuals of both sexes were used for scRNA-seq experiments and flow cytometry studies.

Tissue processing for flow cytometry

Forelimb long bones (humerus, radius and ulna) were dissected from fetuses at embryonic day E18.5 and pups at postnatal day 1 and carefully cleaned of surrounding tissue. Cell suspensions for flow cytometry (FC) analysis or sorting were prepared as previously reported[122], with the following specific modifications. For perinatal stages, bones were cut in small pieces with a scalpel and all tissue was processed (bone marrow cells were not washed out or flushed) for enzymatic digestion using collagenase D (2mg/ml in DMEM [high glucose]). Red cell lysis was not performed. The time of digestion for perinatal stages was 45-50 minutes in a water bath at 37ºC with 3 rounds of gentle pipetting every 10 min to help disaggregation. Collagenase digestion was stopped in ice and by addition of ice-cold 10%FBS/HBSS+ (HBSS, 10mM HEPES, 1% Penicillin-Streptomycin). Cells in suspension were recovered to a new tube and any remaining bone pieces were transferred to a ceramic mortar and 2 to 3 steps of very gentle tapping with the pestle (20-30 times) was applied to increase cell recovery. Cells in the mortar were recovered with the addition of 10%FBS/HBSS+, filtered through a 100μm strainer and pooled with the cell suspension set aside. After centrifugation (350g for 10 min at 4°C), cells were resuspended in 2%FBS/HBSS+ for FC analysis or sorting. Before antibody staining, blocking of FcγR II/III was performed by incubation in ice with anti-CD16/CD32 antibodies for 15 min (1mg/million cells). Collection tubes for sorting were precoated for 15 minutes with 10% FBS/HBSS+ in ice, and kept at 4º C during sorting. Samples were analyzed and sorted in a SONY MA900 (lasers: 488/561 and 405/638nm). 7-AAD (7-amino actinomycin D) was the

only dye used to discriminate dead cells. The lineage cocktail to analyze mesenchymal populations included CD45 (hematopoietic cells), TER119 (erythroid cells) and CD31 (endothelial cells), all conjugated to biotin and detected via secondary staining with Streptavidin-PECy7. Lowly-expressed molecules were stained with antibodies conjugated either with BV421 (not used when PB was selected), PE or APC, while highly expressed molecules were stained with antibodies conjugated either with PB (not used when BV421 was selected), FITC, BV785 or A700 fluorophores. All antibodies used are referenced in Table 1.

Table 1. Antibodies used in this study	**Biolegend Cat. No.**
FITC anti-mouse CD9 (clone MZ3)	124807
Brilliant Violet 421™ anti-mouse CD140a (clone APA5)	135923
APC anti-mouse CD140a (clone APA5)	135907
APC anti-mouse CD31 (clone 390)	102409
Brilliant Violet 785™ anti-mouse Ly-6A/E (Sca-1) (clone D7)	108139
Alexa Fluor 700 anti-mouse CD90.2 (Thy-1.2) (clone 53-2.1)	140323
FITC anti-mouse Podoplanin (clone 8.1.1)	127415
APC anti-mouse CD39 (clone Duha59)	143809
PE anti-mouse CD55 (DAF) (clone RIKO-3)	131803
Biotin anti-mouse TER-119/Erythroid Cells (clone TER-119)	116204
Biotin anti-mouse CD31 (clone 390)	102404
Biotin anti-mouse CD45 (clone 30-F11)	103104

Flow cytometry analysis

Data was acquired with a SONY MA900 using the equipment's software and further analyzed using FlowJo v10.8.0. Representative plots of at least three independent experiments are shown.

Generation of single cell RNA-seq datasets

Five embryos E18.5 and four newborns PN1, all littermates, were processed for cell suspension preparation as described above. No sex discrimination was done since at perinatal stages gender associated differences are not highly relevant. Still, we interrogated gender-related genes such *Xist, Esr1* and *Esr2* (female) and *Ddx3y, Eif2s3y, Kdm5d* and *Uty* (male) [123] in the scRNAseq analysis and observed that both females and males are represented in both stages. After eliminating dead cells and

multiplets by electronical gating, the different fractions of sorted cells (100μm nozzle) were mixed in the proportions detailed in Fig. 1a. Cells were sorted in excess (~5X more than calculated) to account for cell loss. Absence of cell aggregates was confirmed by microscopic visualization, and cell number and viability were assessed in a TC-20 cell counter (Bio-Rad) with trypan blue staining. For both E18.5 and PN1 samples, viability was > 90%. Cells were resuspended in HBSS+ 2%FBS at 800 cells/μl and 20.000 cells were loaded in a Chromium Controller G chip (10x Genomics) and processed with the Chromium Next GEM Single Cell 3' Kit v3.1 for the generation of the scRNAseq libraries in parallel, according to the manufacturer's protocol. Libraries were sequenced on a DNBSEQ-T7 system (PE100/100/10/10; sequencing performed by BGI).

Analysis of single cell RNA-seq datasets

Pre-processing of scRNAseq data. Reads were aligned to the mouse genome (mm10) with the Cell Ranger v6.0 software. Cells with fewer than 400 or more than 6,000 detected genes, or more than 10% of mitochondrial reads were excluded. For normalization, log-transformation with a scale factor of 10,000 was used.

Dimensional reduction and clustering. 2,000 top high variable genes (HVG) were identified with the "vst" method of the *FindVariableFeatures* function of the Seurat package (version 4.0.3[124]). The data were scaled and PCA (30 PCs) performed. The cells were clustered using the Louvain Method on a nearest neighbor graph using the *FindClusters* and *FindNeighbors* in Seurat. A UMAP on the PCA reduced data was performed to visualize the clusters.

Elimination of erythroid cells and doublets. Based on gene markers, erythroid cells were removed from downstream analyses. For doublet removal, the software DoubletFinder[125] was used. After filtering low-quality cells, putative doublets and erythroid cells, our dataset contained 7,272 cells with 10,656 mean number of reads and 2,625 mean number of genes for E18.5 and 7,277 cells with 9,827 mean number of reads and 2,533 mean number of genes in PN1.

Sample integration. In order to jointly analyze both E18.5 and PN1 samples, data were integrated with the Harmony software[39] and projected into a shared 2D UMAP embedding. Perinatal samples were then integrated with the adult dataset from Baccin

et al.[21]. The adult data is available to download as a Seurat object from https://nicheview.shiny.embl.de.

Cell type annotation. Marker genes described in the extensive literature were used for cluster identification. Although most of the cell types were annotated using a given clustering resolution, subsequent refinement was done through sub-clustering (*FindSubCluster* function of Seurat) and re-annotation.

Analysis of the mesenchymal compartment. Mesenchymal clusters were extracted and reprocessed as before (i.e. HVG, PCA, clustering, UMAP). The PHATE algorithm[55] was used to investigate the main developmental branches in the mesenchymal compartment (phateR package version 1.0.7 available in CRAN).

Inference of cell-cell interactions. CellPhoneDB v.2[57] was used to infer cell-cell connections. To prepare the data for the CellPhoneDB analysis, mouse gene IDs were converted to their human orthologs and count data exported as h5ad format. CellPhoneDB statistical analysis was used to evaluate for significant interactions between predefined cell type pairs. For direct interactions, we considered only connector with no secreted molecules and p-val < 0.05 and Log2 mean > -1. Chord representations were generated using the ktplots R package version 1.2.3 (https://doi.org/10.5281/zenodo.7699617).

Gene Regulatory Network analysis. Inference of gene regulatory networks and regulon analysis was performed using the pySCENIC software v.0.11.2[78].

Gene ontology analysis

Genes lists for each of the mesenchymal GFP, SFP, AFP and CLFP clusters at E18.5 and PN1 were retrieved (log2 fold-change> 0.5 [1.4 fold increase] and adjusted p-value < 0.05, as calculated by the Cell Ranger software). GO terms for the “Biological Process” category were retrieved from http://geneontology.org, filtered by a ratio Fold Enriched/Expected> 2 and manually curated. Plots were generated using the ggplot2 tool for R, representing the -log10 (p values < 0.05), and the overlap was calculated using the number of genes identified in the GO term for each cluster.

DATA AND CODE AVAILABILITY

- Single-cell RNA-seq data have been deposited in the GEO database (accession number GSE232202) and are publicly available as of the date of publication. Flow cytometry data reported in this paper will be shared by the corresponding authors upon request.
- All scripts necessary to replicate our analysis are available in the following Github repository (https://github.com/irepansalvador/stromal_cells.git) and is publicly available as of the date of publication.

ACKNOWLEDGMENTS

We thank the rest of the members of the groups for scientific discussions and technical help. We are also grateful to A. Franco, C. Mateos, A. López, P. López and L. Pérez for excellent mouse husbrandy as well as the rest of the CABD Core services, in particular C. Díaz (Flow Cytometry Facility) and K. García (Microscopy Facility). This work was supported by the Junta de Andalucía (PY20-00421) to J.L-R and the Spanish Ministerio de Ciencia e Innovación María de Maeztu Institutional Grant (CEX2020-001088-M) to J.L-R and J.J.T.

CONFLICT OF INTERESTS

The authors declare no competing interests.

CONTRIBUTIONS

Conceptualization, G.N and J.L-R; Software, I.S.M and I.C; Formal Analysis, G.N, I.S.M, A.D.R, and J.J.T.; Investigation, G.N, A.D.R., I.S-A, A.A.C, A.F-M, A. M, A.M.B. and J.L-R; Writing – Original Draft, G.N, and J.L-R.; Writing – Review & Editing, all authors; Supervision, H.H, J.J.T, J.L-R., and G.N.; Funding Acquisition, H.H, J.J.T, J.L-R., and G.N.

REFERENCES

1 Liggins, G. C. The role of cortisol in preparing the fetus for birth. *Reprod Fertil Dev* **6**, 141-150, doi:10.1071/rd9940141 (1994).

2 Hillman, N. H., Kallapur, S. G. & Jobe, A. H. Physiology of transition from intrauterine to extrauterine life. *Clin Perinatol* **39**, 769-783, doi:10.1016/j.clp.2012.09.009 (2012).

3 Morton, S. U. & Brodsky, D. Fetal Physiology and the Transition to Extrauterine Life. *Clin Perinatol* **43**, 395-407, doi:10.1016/j.clp.2016.04.001 (2016).

4 Sanidad, K. Z. & Zeng, M. Y. Neonatal gut microbiome and immunity. *Curr Opin Microbiol* **56**, 30-37, doi:10.1016/j.mib.2020.05.011 (2020).

5 Bianco, P. & Robey, P. G. Skeletal stem cells. *Development* **142**, 1023-1027, doi:10.1242/dev.102210 (2015).

6 Long, F. & Ornitz, D. M. Development of the endochondral skeleton. *Cold Spring Harb Perspect Biol* **5**, a008334, doi:10.1101/cshperspect.a008334 (2013).

7 Haraguchi, R. *et al.* Recent Insights into Long Bone Development: Central Role of Hedgehog Signaling Pathway in Regulating Growth Plate. *Int J Mol Sci* **20**, doi:10.3390/ijms20235840 (2019).

8 Galea, G. L., Zein, M. R., Allen, S. & Francis-West, P. Making and shaping endochondral and intramembranous bones. *Dev Dyn* **250**, 414-449, doi:10.1002/dvdy.278 (2021).

9 Comazzetto, S., Shen, B. & Morrison, S. J. Niches that regulate stem cells and hematopoiesis in adult bone marrow. *Dev Cell* **56**, 1848-1860, doi:10.1016/j.devcel.2021.05.018 (2021).

10 Jeffery, E. C., Mann, T. L. A., Pool, J. A., Zhao, Z. & Morrison, S. J. Bone marrow and periosteal skeletal stem/progenitor cells make distinct contributions to bone maintenance and repair. *Cell Stem Cell* **29**, 1547-1561 e1546, doi:10.1016/j.stem.2022.10.002 (2022).

11 Shu, H. S. *et al.* Tracing the skeletal progenitor transition during postnatal bone formation. *Cell Stem Cell* **28**, 2122-2136 e2123, doi:10.1016/j.stem.2021.08.010 (2021).

12 Li, Q., Xu, R., Lei, K. & Yuan, Q. Insights into skeletal stem cells. *Bone Res* **10**, 61, doi:10.1038/s41413-022-00235-8 (2022).

13 Zhou, X. *et al.* Chondrocytes transdifferentiate into osteoblasts in endochondral bone during development, postnatal growth and fracture healing in mice. *PLoS Genet* **10**, e1004820, doi:10.1371/journal.pgen.1004820 (2014).

14 Yang, L., Tsang, K. Y., Tang, H. C., Chan, D. & Cheah, K. S. Hypertrophic chondrocytes can become osteoblasts and osteocytes in endochondral bone formation. *Proc Natl Acad Sci U S A* **111**, 12097-12102, doi:10.1073/pnas.1302703111 (2014).

15 Hallett, S. A., Ono, W. & Ono, N. The hypertrophic chondrocyte: To be or not to be. *Histol Histopathol* **36**, 1021-1036, doi:10.14670/HH-18-355 (2021).

16 Johnson, G. L., Masias, E. J. & Lehoczky, J. A. Cellular Heterogeneity and Lineage Restriction during Mouse Digit Tip Regeneration at Single-Cell Resolution. *Dev Cell* **52**, 525-540 e525, doi:10.1016/j.devcel.2020.01.026 (2020).

17 Storer, M. A. *et al.* Acquisition of a Unique Mesenchymal Precursor-like Blastema State Underlies Successful Adult Mammalian Digit Tip Regeneration. *Dev Cell* **52**, 509-524 e509, doi:10.1016/j.devcel.2019.12.004 (2020).

18 Lin, T. Y. *et al.* Fibroblast dedifferentiation as a determinant of successful regeneration. *Dev Cell* **56**, 1541-1551 e1546, doi:10.1016/j.devcel.2021.04.016 (2021).

19 Newton, P. T. *et al.* A radical switch in clonality reveals a stem cell niche in the epiphyseal growth plate. *Nature* **567**, 234-238, doi:10.1038/s41586-019-0989-6 (2019).

20 Matsushita, Y., Ono, W. & Ono, N. Bone regeneration via skeletal cell lineage plasticity: All hands mobilized for emergencies: Quiescent mature skeletal cells can be activated in response to injury and robustly participate in bone regeneration through cellular plasticity. *Bioessays* **43**, e2000202, doi:10.1002/bies.202000202 (2021).

21 Baccin, C. *et al.* Combined single-cell and spatial transcriptomics reveal the molecular, cellular and spatial bone marrow niche organization. *Nat Cell Biol* **22**, 38-48, doi:10.1038/s41556-019-0439-6 (2020).

22 Buenrostro, J. D. *et al.* Integrated Single-Cell Analysis Maps the Continuous Regulatory Landscape of Human Hematopoietic Differentiation. *Cell* **173**, 1535-1548 e1516, doi:10.1016/j.cell.2018.03.074 (2018).

23 Triana, S. *et al.* Single-cell proteo-genomic reference maps of the hematopoietic system enable the purification and massive profiling of precisely defined cell states. *Nat Immunol* **22**, 1577-1589, doi:10.1038/s41590-021-01059-0 (2021).

24 Ranzoni, A. M. *et al.* Integrative Single-Cell RNA-Seq and ATAC-Seq Analysis of Human Developmental Hematopoiesis. *Cell Stem Cell* **28**, 472-487 e477, doi:10.1016/j.stem.2020.11.015 (2021).

25 Akiyama, H. & Lefebvre, V. Unraveling the transcriptional regulatory machinery in chondrogenesis. *J Bone Miner Metab* **29**, 390-395, doi:10.1007/s00774-011-0273-9 (2011).

26 Komori, T. Whole Aspect of Runx2 Functions in Skeletal Development. *Int J Mol Sci* **23**, doi:10.3390/ijms23105776 (2022).

27 Alonso-Martin, S. *et al.* Gene Expression Profiling of Muscle Stem Cells Identifies Novel Regulators of Postnatal Myogenesis. *Front Cell Dev Biol* **4**, 58, doi:10.3389/fcell.2016.00058 (2016).

28 Murchison, N. D. *et al.* Regulation of tendon differentiation by scleraxis distinguishes force-transmitting tendons from muscle-anchoring tendons. *Development* **134**, 2697-2708, doi:10.1242/dev.001933 (2007).

29 Shukunami, C. *et al.* Scleraxis is a transcriptional activator that regulates the expression of Tenomodulin, a marker of mature tenocytes and ligamentocytes. *Sci Rep* **8**, 3155, doi:10.1038/s41598-018-21194-3 (2018).

30 Rees, S. G. *et al.* Immunolocalisation and expression of keratocan in tendon. *Osteoarthritis Cartilage* **17**, 276-279, doi:10.1016/j.joca.2008.07.007 (2009).

31 Zhang, Y. *et al.* Generation and Characterization of a Novel Mouse Line, Keratocan-rtTA (KeraRT), for Corneal Stroma and Tendon Research. *Invest Ophthalmol Vis Sci* **58**, 4800-4808, doi:10.1167/iovs.17-22661 (2017).

32 Jelinsky, S. A., Archambault, J., Li, L. & Seeherman, H. Tendon-selective genes identified from rat and human musculoskeletal tissues. *J Orthop Res* **28**, 289-297, doi:10.1002/jor.20999 (2010).

33 Pacifici, M., Koyama, E., Iwamoto, M. & Gentili, C. Development of articular cartilage: what do we know about it and how may it occur? *Connect Tissue Res* **41**, 175-184, doi:10.3109/03008200009005288 (2000).

34 Chijimatsu, R. & Saito, T. Mechanisms of synovial joint and articular cartilage development. *Cell Mol Life Sci* **76**, 3939-3952, doi:10.1007/s00018-019-03191-5 (2019).

35 Eschenbrenner, E. *et al.* TspanC8 tetraspanins differentially regulate ADAM10 endocytosis and half-life. *Life Sci Alliance* **3**, doi:10.26508/lsa.201900444 (2020).

36 Mizuno, S. *et al.* ADAM10 is indispensable for longitudinal bone growth in mice. *Bone* **134**, 115273, doi:10.1016/j.bone.2020.115273 (2020).

37 Lima, I. L. A. *et al.* Contribution of atypical chemokine receptor 2/ackr2 in bone remodeling. *Bone* **101**, 113-122, doi:10.1016/j.bone.2017.05.003 (2017).

38 Decker, R. S. *et al.* Cell origin, volume and arrangement are drivers of articular cartilage formation, morphogenesis and response to injury in mouse limbs. *Dev Biol* **426**, 56-68, doi:10.1016/j.ydbio.2017.04.006 (2017).

39 Korsunsky, I. *et al.* Fast, sensitive and accurate integration of single-cell data with Harmony. *Nat Methods* **16**, 1289-1296, doi:10.1038/s41592-019-0619-0 (2019).

40 Luecken, M. D. *et al.* Benchmarking atlas-level data integration in single-cell genomics. *Nat Methods* **19**, 41-50, doi:10.1038/s41592-021-01336-8 (2022).

41 Sugiyama, T., Kohara, H., Noda, M. & Nagasawa, T. Maintenance of the hematopoietic stem cell pool by CXCL12-CXCR4 chemokine signaling in bone marrow stromal cell niches. *Immunity* **25**, 977-988, doi:10.1016/j.immuni.2006.10.016 (2006).

42 Morrison, S. J. & Scadden, D. T. The bone marrow niche for haematopoietic stem cells. *Nature* **505**, 327-334, doi:10.1038/nature12984 (2014).

43 Ding, L., Saunders, T. L., Enikolopov, G. & Morrison, S. J. Endothelial and perivascular cells maintain haematopoietic stem cells. *Nature* **481**, 457-462, doi:10.1038/nature10783 (2012).

44 Ding, L. & Morrison, S. J. Haematopoietic stem cells and early lymphoid progenitors occupy distinct bone marrow niches. *Nature* **495**, 231-235, doi:10.1038/nature11885 (2013).

45 Wolock, S. L. *et al.* Mapping Distinct Bone Marrow Niche Populations and Their Differentiation Paths. *Cell Rep* **28**, 302-311 e305, doi:10.1016/j.celrep.2019.06.031 (2019).

46 Tikhonova, A. N. *et al.* The bone marrow microenvironment at single-cell resolution. *Nature* **569**, 222-228, doi:10.1038/s41586-019-1104-8 (2019).

47 Matsushita, Y. *et al.* A Wnt-mediated transformation of the bone marrow stromal cell identity orchestrates skeletal regeneration. *Nat Commun* **11**, 332, doi:10.1038/s41467-019-14029-w (2020).

48 Mo, C. *et al.* Single-cell transcriptomics of LepR-positive skeletal cells reveals heterogeneous stress-dependent stem and progenitor pools. *EMBO J* **41**, e108415, doi:10.15252/embj.2021108415 (2022).

49 Severe, N. *et al.* Stress-Induced Changes in Bone Marrow Stromal Cell Populations Revealed through Single-Cell Protein Expression Mapping. *Cell Stem Cell* **25**, 570-583 e577, doi:10.1016/j.stem.2019.06.003 (2019).

50 Mizoguchi, T. *et al.* Osterix marks distinct waves of primitive and definitive stromal progenitors during bone marrow development. *Dev Cell* **29**, 340-349, doi:10.1016/j.devcel.2014.03.013 (2014).

51 Kara, N. *et al.* Endothelial and Leptin Receptor(+) cells promote the maintenance of stem cells and hematopoiesis in early postnatal murine bone marrow. *Dev Cell* **58**, 348-360 e346, doi:10.1016/j.devcel.2023.02.003 (2023).

52 Baryawno, N. *et al.* A Cellular Taxonomy of the Bone Marrow Stroma in Homeostasis and Leukemia. *Cell* **177**, 1915-1932 e1916, doi:10.1016/j.cell.2019.04.040 (2019).

53 Matthews, B. G. *et al.* Heterogeneity of murine periosteum progenitors involved in fracture healing. *Elife* **10**, doi:10.7554/eLife.58534 (2021).

54 Chan, C. K. *et al.* Identification and specification of the mouse skeletal stem cell. *Cell* **160**, 285-298, doi:10.1016/j.cell.2014.12.002 (2015).

55 Moon, K. R. *et al.* Visualizing structure and transitions in high-dimensional biological data. *Nat Biotechnol* **37**, 1482-1492, doi:10.1038/s41587-019-0336-3 (2019).

56 Li, Z. *et al.* Lipolysis of bone marrow adipocytes is required to fuel bone and the marrow niche during energy deficits. *Elife* **11**, doi:10.7554/eLife.78496 (2022).

57 Efremova, M., Vento-Tormo, M., Teichmann, S. A. & Vento-Tormo, R. CellPhoneDB: inferring cell-cell communication from combined expression of multi-subunit ligand-receptor complexes. *Nat Protoc* **15**, 1484-1506, doi:10.1038/s41596-020-0292-x (2020).

58 Helbling, P. M. *et al.* Global Transcriptomic Profiling of the Bone Marrow Stromal Microenvironment during Postnatal Development, Aging, and Inflammation. *Cell Rep* **29**, 3313-3330 e3314, doi:10.1016/j.celrep.2019.11.004 (2019).

59 Carver, W., Molano, I., Reaves, T. A., Borg, T. K. & Terracio, L. Role of the alpha 1 beta 1 integrin complex in collagen gel contraction in vitro by fibroblasts. *J Cell Physiol* **165**, 425-437, doi:10.1002/jcp.1041650224 (1995).

60 Ylonen, R. *et al.* Type XIII collagen strongly affects bone formation in transgenic mice. *J Bone Miner Res* **20**, 1381-1393, doi:10.1359/JBMR.050319 (2005).

61 Kemppainen, A. V. *et al.* The CMS19 disease model specifies a pivotal role for collagen XIII in bone homeostasis. *Sci Rep* **12**, 5866, doi:10.1038/s41598-022-09653-4 (2022).

62 Long, K. R. & Huttner, W. B. How the extracellular matrix shapes neural development. *Open Biol* **9**, 180216, doi:10.1098/rsob.180216 (2019).

63 Stone, A. *et al.* Extracellular matrices of bone marrow stroma regulate cell phenotype and contribute to distinct stromal niches in vivo. *bioRxiv*, 2023.2001.2019.524473, doi:10.1101/2023.01.19.524473 (2023).

64 Zieba, J. T., Chen, Y. T., Lee, B. H. & Bae, Y. Notch Signaling in Skeletal Development, Homeostasis and Pathogenesis. *Biomolecules* **10**, doi:10.3390/biom10020332 (2020).

65 Gonzalez, M. J. *et al.* DLK1 is a novel inflammatory inhibitor which interferes with NOTCH1 signaling in TLR-activated murine macrophages. *Eur J Immunol* **45**, 2615-2627, doi:10.1002/eji.201545514 (2015).

66 Rebelo, A. P. *et al.* A CADM3 variant causes Charcot-Marie-Tooth disease with marked upper limb involvement. *Brain* **144**, 1197-1213, doi:10.1093/brain/awab019 (2021).

67 Johnston, A. P. Schwann cells: an emerging player in tissue regeneration. *Stem Cell Investig* **4**, 14, doi:10.21037/sci.2017.02.05 (2017).

68 Di Rosa, F. & Gebhardt, T. Bone Marrow T Cells and the Integrated Functions of Recirculating and Tissue-Resident Memory T Cells. *Front Immunol* **7**, 51, doi:10.3389/fimmu.2016.00051 (2016).

69 Shan, Q. *et al.* Tcf1 and Lef1 provide constant supervision to mature CD8(+) T cell identity and function by organizing genomic architecture. *Nat Commun* **12**, 5863, doi:10.1038/s41467-021-26159-1 (2021).

70 Jung, Y. W., Kim, H. G., Perry, C. J. & Kaech, S. M. CCR7 expression alters memory CD8 T-cell homeostasis by regulating occupancy in IL-7- and IL-15-dependent niches. *Proc Natl Acad Sci U S A* **113**, 8278-8283, doi:10.1073/pnas.1602899113 (2016).

71 Liu, C., Lan, Y., Liu, B., Zhang, H. & Hu, H. T Cell Development: Old Tales Retold By Single-Cell RNA Sequencing. *Trends Immunol* **42**, 165-175, doi:10.1016/j.it.2020.12.004 (2021).

72 Lavaert, M. *et al.* Integrated scRNA-Seq Identifies Human Postnatal Thymus Seeding Progenitors and Regulatory Dynamics of Differentiating Immature Thymocytes. *Immunity* **52**, 1088-1104 e1086, doi:10.1016/j.immuni.2020.03.019 (2020).

73 Rothenberg, E. V. Single-cell insights into the hematopoietic generation of T-lymphocyte precursors in mouse and human. *Exp Hematol* **95**, 1-12, doi:10.1016/j.exphem.2020.12.005 (2021).

74 Ortinau, L. C. *et al.* Identification of Functionally Distinct Mx1+alphaSMA+ Periosteal Skeletal Stem Cells. *Cell Stem Cell* **25**, 784-796 e785, doi:10.1016/j.stem.2019.11.003 (2019).

75 Cumano, A. *et al.* New Molecular Insights into Immune Cell Development. *Annu Rev Immunol* **37**, 497-519, doi:10.1146/annurev-immunol-042718-041319 (2019).

76 Zeng, Y. *et al.* Single-Cell RNA Sequencing Resolves Spatiotemporal Development of Pre-thymic Lymphoid Progenitors and Thymus Organogenesis in Human Embryos. *Immunity* **51**, 930-948 e936, doi:10.1016/j.immuni.2019.09.008 (2019).

77 Aibar, S. *et al.* SCENIC: single-cell regulatory network inference and clustering. *Nat Methods* **14**, 1083-1086, doi:10.1038/nmeth.4463 (2017).

78 Van de Sande, B. *et al.* A scalable SCENIC workflow for single-cell gene regulatory network analysis. *Nat Protoc* **15**, 2247-2276, doi:10.1038/s41596-020-0336-2 (2020).

79 Rao, J. *et al.* Reconstructing human Brown Fat developmental trajectory in vitro. *bioRxiv*, 2022.2006.2001.494355, doi:10.1101/2022.06.01.494355 (2022).

80 Hu, Y. *et al.* Identification of Novel Potentially Pleiotropic Variants Associated With Osteoporosis and Obesity Using the cFDR Method. *J Clin Endocrinol Metab* **103**, 125-138, doi:10.1210/jc.2017-01531 (2018).

81 Seale, P. *et al.* PRDM16 controls a brown fat/skeletal muscle switch. *Nature* **454**, 961-967, doi:10.1038/nature07182 (2008).

82 Van Nguyen, T. T., Vu, V. V. & Pham, P. V. Transcriptional Factors of Thermogenic Adipocyte Development and Generation of Brown and Beige Adipocytes From Stem Cells. *Stem Cell Rev Rep* **16**, 876-892, doi:10.1007/s12015-020-10013-w (2020).

83 Liu, H. *et al.* Mohawk promotes the tenogenesis of mesenchymal stem cells through activation of the TGFbeta signaling pathway. *Stem Cells* **33**, 443-455, doi:10.1002/stem.1866 (2015).

84 Milet, C. & Duprez, D. The Mkx homeoprotein promotes tenogenesis in stem cells and improves tendon repair. *Ann Transl Med* **3**, S33, doi:10.3978/j.issn.2305-5839.2015.03.64 (2015).

85 Mallo, M. Reassessing the Role of Hox Genes during Vertebrate Development and Evolution. *Trends Genet* **34**, 209-217, doi:10.1016/j.tig.2017.11.007 (2018).

86 Rux, D. R. *et al.* Regionally Restricted Hox Function in Adult Bone Marrow Multipotent Mesenchymal Stem/Stromal Cells. *Dev Cell* **39**, 653-666, doi:10.1016/j.devcel.2016.11.008 (2016).

87 Cartwright, T., Perkins, N. D. & C, L. W. NFKB1: a suppressor of inflammation, ageing and cancer. *FEBS J* **283**, 1812-1822, doi:10.1111/febs.13627 (2016).

88 Wessells, J. *et al.* BCL-3 and NF-kappaB p50 attenuate lipopolysaccharide-induced inflammatory responses in macrophages. *J Biol Chem* **279**, 49995-50003, doi:10.1074/jbc.M404246200 (2004).

89 Hai, T., Wolford, C. C. & Chang, Y. S. ATF3, a hub of the cellular adaptive-response network, in the pathogenesis of diseases: is modulation of inflammation a unifying component? *Gene Expr* **15**, 1-11, doi:10.3727/105221610x12819686555015 (2010).

90 Kwon, J. W. *et al.* Activating transcription factor 3 represses inflammatory responses by binding to the p65 subunit of NF-kappaB. *Sci Rep* **5**, 14470, doi:10.1038/srep14470 (2015).

91 Knights, A. J. *et al.* Kruppel-like factor 3 (KLF3) suppresses NF-kappaB-driven inflammation in mice. *J Biol Chem* **295**, 6080-6091, doi:10.1074/jbc.RA120.013114 (2020).

92 Abe, M., Saeki, N., Ikeda, Y. & Ohba, S. Kruppel-like Factors in Skeletal Physiology and Pathologies. *Int J Mol Sci* **23**, doi:10.3390/ijms232315174 (2022).

93 Ghaleb, A. M. & Yang, V. W. Kruppel-like factor 4 (KLF4): What we currently know. *Gene* **611**, 27-37, doi:10.1016/j.gene.2017.02.025 (2017).

94 Liao, X. *et al.* Kruppel-like factor 4 regulates macrophage polarization. *J Clin Invest* **121**, 2736-2749, doi:10.1172/JCI45444 (2011).

95 Kawata, M. *et al.* Kruppel-like factor-4 and Kruppel-like factor-2 are important regulators of joint tissue cells and protect against tissue destruction and inflammation in osteoarthritis. *Ann Rheum Dis*, doi:10.1136/annrheumdis-2021-221867 (2022).

96 Choi, S. *et al.* Kruppel-Like Factor 4 Positively Regulates Autoimmune Arthritis in Mouse Models and Rheumatoid Arthritis in Patients via Modulating Cell

Survival and Inflammation Factors of Fibroblast-Like Synoviocyte. *Front Immunol* **9**, 1339, doi:10.3389/fimmu.2018.01339 (2018).

97 Li, C., Yu, L., Mai, C., Mu, T. & Zeng, Y. KLF4 down-regulation resulting from TLR4 promotion of ERK1/2 phosphorylation underpins inflammatory response in sepsis. *J Cell Mol Med* **25**, 2013-2024, doi:10.1111/jcmm.16082 (2021).

98 Balamurugan, K. & Sterneck, E. The many faces of C/EBPdelta and their relevance for inflammation and cancer. *Int J Biol Sci* **9**, 917-933, doi:10.7150/ijbs.7224 (2013).

99 Moore, F. *et al.* The transcription factor C/EBP delta has anti-apoptotic and anti-inflammatory roles in pancreatic beta cells. *PLoS One* **7**, e31062, doi:10.1371/journal.pone.0031062 (2012).

100 Rustenhoven, J. *et al.* An anti-inflammatory role for C/EBPdelta in human brain pericytes. *Sci Rep* **5**, 12132, doi:10.1038/srep12132 (2015).

101 Scheiermann, C., Kunisaki, Y. & Frenette, P. S. Circadian control of the immune system. *Nat Rev Immunol* **13**, 190-198, doi:10.1038/nri3386 (2013).

102 Curtis, A. M., Bellet, M. M., Sassone-Corsi, P. & O'Neill, L. A. Circadian clock proteins and immunity. *Immunity* **40**, 178-186, doi:10.1016/j.immuni.2014.02.002 (2014).

103 Liu, H. *et al.* NR1D1 modulates synovial inflammation and bone destruction in rheumatoid arthritis. *Cell Death Dis* **11**, 129, doi:10.1038/s41419-020-2314-6 (2020).

104 Pai, P. & Sukumar, S. HOX genes and the NF-kappaB pathway: A convergence of developmental biology, inflammation and cancer biology. *Biochim Biophys Acta Rev Cancer* **1874**, 188450, doi:10.1016/j.bbcan.2020.188450 (2020).

105 Mucientes, A. *et al.* Differential Expression of HOX Genes in Mesenchymal Stem Cells from Osteoarthritic Patients Is Independent of Their Promoter Methylation. *Cells* **7**, doi:10.3390/cells7120244 (2018).

106 Morikawa, S. *et al.* Prospective identification, isolation, and systemic transplantation of multipotent mesenchymal stem cells in murine bone marrow. *J Exp Med* **206**, 2483-2496, doi:10.1084/jem.20091046 (2009).

107 Nusspaumer, G. *et al.* Ontogenic Identification and Analysis of Mesenchymal Stromal Cell Populations during Mouse Limb and Long Bone Development. *Stem Cell Reports* **9**, 1124-1138, doi:10.1016/j.stemcr.2017.08.007 (2017).

108 Ambrosi, T. H. *et al.* Adipocyte Accumulation in the Bone Marrow during Obesity and Aging Impairs Stem Cell-Based Hematopoietic and Bone Regeneration. *Cell Stem Cell* **20**, 771-784 e776, doi:10.1016/j.stem.2017.02.009 (2017).

109 Ambrosi, T. H. *et al.* Distinct skeletal stem cell types orchestrate long bone skeletogenesis. *Elife* **10**, doi:10.7554/eLife.66063 (2021).

110 Duchamp de Lageneste, O. *et al.* Periosteum contains skeletal stem cells with high bone regenerative potential controlled by Periostin. *Nat Commun* **9**, 773, doi:10.1038/s41467-018-03124-z (2018).

111 Perrin, S. *et al.* Periosteal response to bone fracture at single nuclei resolution. *bioRxiv*, 2023.2006.2023.546220, doi:10.1101/2023.06.23.546220 (2023).

112 Guarnerio, J. *et al.* Bone marrow endosteal mesenchymal progenitors depend on HIF factors for maintenance and regulation of hematopoiesis. *Stem Cell Reports* **2**, 794-809, doi:10.1016/j.stemcr.2014.04.002 (2014).

113 Lee, P. Y., Wang, J. X., Parisini, E., Dascher, C. C. & Nigrovic, P. A. Ly6 family proteins in neutrophil biology. *J Leukoc Biol* **94**, 585-594, doi:10.1189/jlb.0113014 (2013).

114 Gomariz, A. *et al.* Quantitative spatial analysis of haematopoiesis-regulating stromal cells in the bone marrow microenvironment by 3D microscopy. *Nat Commun* **9**, 2532, doi:10.1038/s41467-018-04770-z (2018).

115 Omatsu, Y. *et al.* The essential functions of adipo-osteogenic progenitors as the hematopoietic stem and progenitor cell niche. *Immunity* **33**, 387-399, doi:10.1016/j.immuni.2010.08.017 (2010).

116 Sakaguchi, S., Takahashi, T. & Nishizuka, Y. Study on cellular events in post-thymectomy autoimmune oophoritis in mice. II. Requirement of Lyt-1 cells in normal female mice for the prevention of oophoritis. *J Exp Med* **156**, 1577-1586, doi:10.1084/jem.156.6.1577 (1982).

117 Yang, S., Fujikado, N., Kolodin, D., Benoist, C. & Mathis, D. Immune tolerance. Regulatory T cells generated early in life play a distinct role in maintaining self-tolerance. *Science* **348**, 589-594, doi:10.1126/science.aaa7017 (2015).

118 Ferreirinha, P., Pinheiro, R. G. R., Landry, J. J. M. & Alves, N. L. Identification of fibroblast progenitors in the developing mouse thymus. *Development* **149**, doi:10.1242/dev.200513 (2022).

119 Dhakal, M., Miller, M. M., Zaghouani, A. A., Sherman, M. P. & Zaghouani, H. Neonatal Basophils Stifle the Function of Early-Life Dendritic Cells To Curtail Th1 Immunity in Newborn Mice. *J Immunol* **195**, 507-518, doi:10.4049/jimmunol.1500027 (2015).

120 Luo, Y. *et al.* Expected impact of immunomodulatory agents during pregnancy: A newborn's perspective. *Pediatr Allergy Immunol* **34**, e13911, doi:10.1111/pai.13911 (2023).

121 Ho, N. P. & Takizawa, H. Inflammation Regulates Haematopoietic Stem Cells and Their Niche. *Int J Mol Sci* **23**, doi:10.3390/ijms23031125 (2022).

122 Houlihan, D. D. *et al.* Isolation of mouse mesenchymal stem cells on the basis of expression of Sca-1 and PDGFR-alpha. *Nat Protoc* **7**, 2103-2111, doi:10.1038/nprot.2012.125 (2012).

123 Shay, D. A. *et al.* Changes in nucleus accumbens gene expression accompany sex-specific suppression of spontaneous physical activity in aromatase knockout mice. *Horm Behav* **121**, 104719, doi:10.1016/j.yhbeh.2020.104719 (2020).

124 Hao, Y. *et al.* Integrated analysis of multimodal single-cell data. *Cell* **184**, 3573-3587 e3529, doi:10.1016/j.cell.2021.04.048 (2021).

125 McGinnis, C. S., Murrow, L. M. & Gartner, Z. J. DoubletFinder: Doublet Detection in Single-Cell RNA Sequencing Data Using Artificial Nearest Neighbors. *Cell Syst* **8**, 329-337 e324, doi:10.1016/j.cels.2019.03.003 (2019).

FIGURE 1

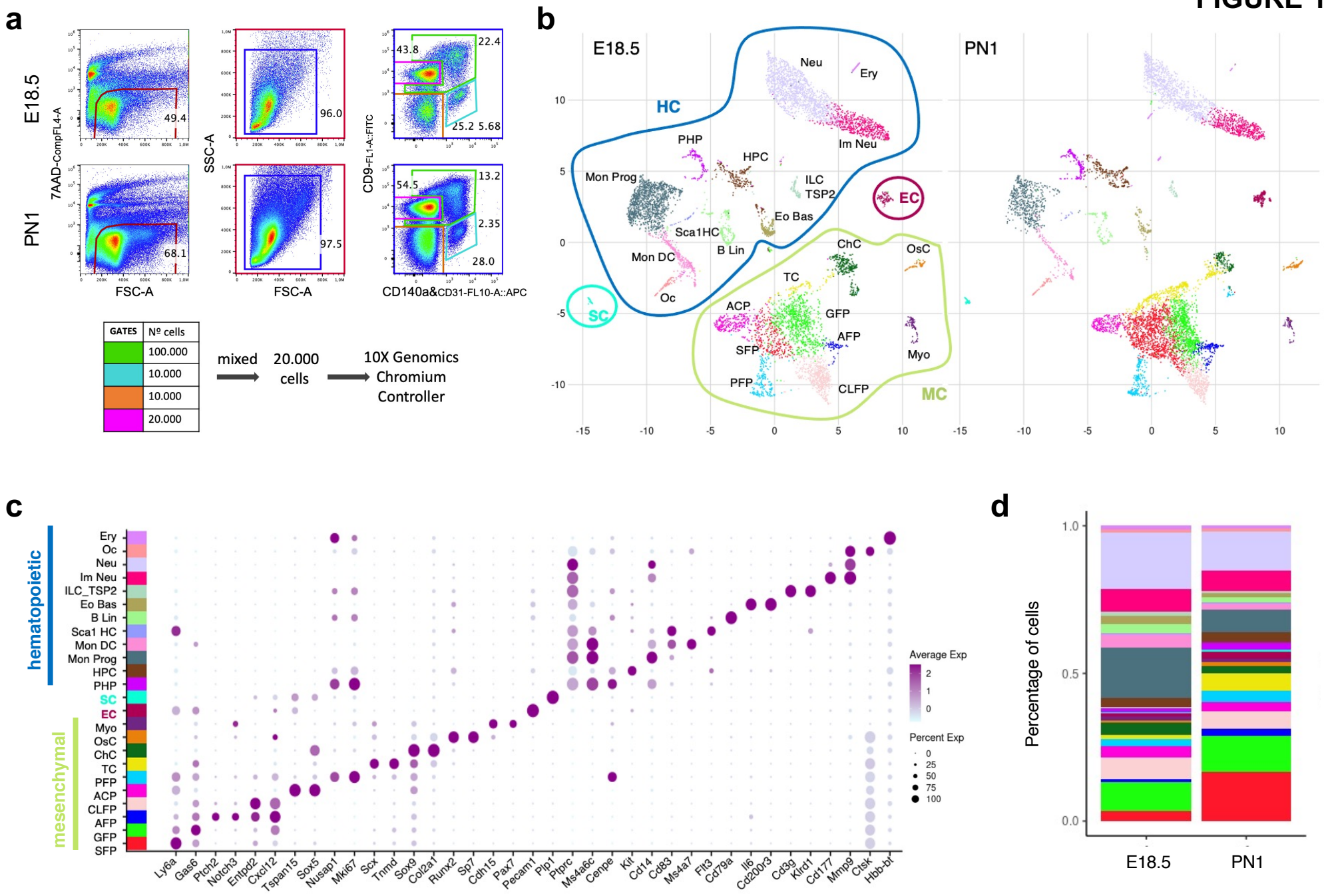
a
E18.5
PN1
7AAD-CompFL4-A
FSC-A
49.4
68.1
SSC-A
96.0
97.5
CD9-FL1-A::FITC
CD140a&CD31-FL10-A::APC
43.8
22.4
25.2
5.68
54.5
13.2
2.35
28.0
GATES
Nº cells
100.000
10.000
10.000
20.000
mixed
20.000 cells
10X Genomics Chromium Controller
b
E18.5
PN1
HC
SC
EC
MC
Neu
Ery
Im Neu
PHP
HPC
Mon Prog
ILC
TSP2
Eo Bas
Sca1HC
B Lin
Mon DC
Oc
ChC
OsC
TC
ACP
GFP
AFP
SFP
Myo
PFP
CLFP
c
hematopoietic
mesenchymal
Ery
Oc
Neu
Im Neu
ILC_TSP2
Eo Bas
B Lin
Sca1 HC
Mon DC
Mon Prog
HPC
PHP
SC
EC
Myo
OsC
ChC
TC
PFP
ACP
CLFP
AFP
GFP
SFP
Ly6a
Gas6
Ptch2
Notch3
Entpd2
Cxcl12
Tspan15
Sox5
Nusap1
Mki67
Scx
Tnmd
Sox9
Col2a1
Runx2
Sp7
Cdh15
Pax7
Pecam1
Plp1
Ptprc
Ms4a6c
Cenpe
Kit
Cd14
Cd83
Ms4a7
Flt3
Cd79a
Il6
Cd200r3
Cd3g
Klrd1
Cd177
Mmp9
Ctsk
Hbb-bt
Average Exp
Percent Exp
d
Percentage of cells
E18.5
PN1

FIGURE 2

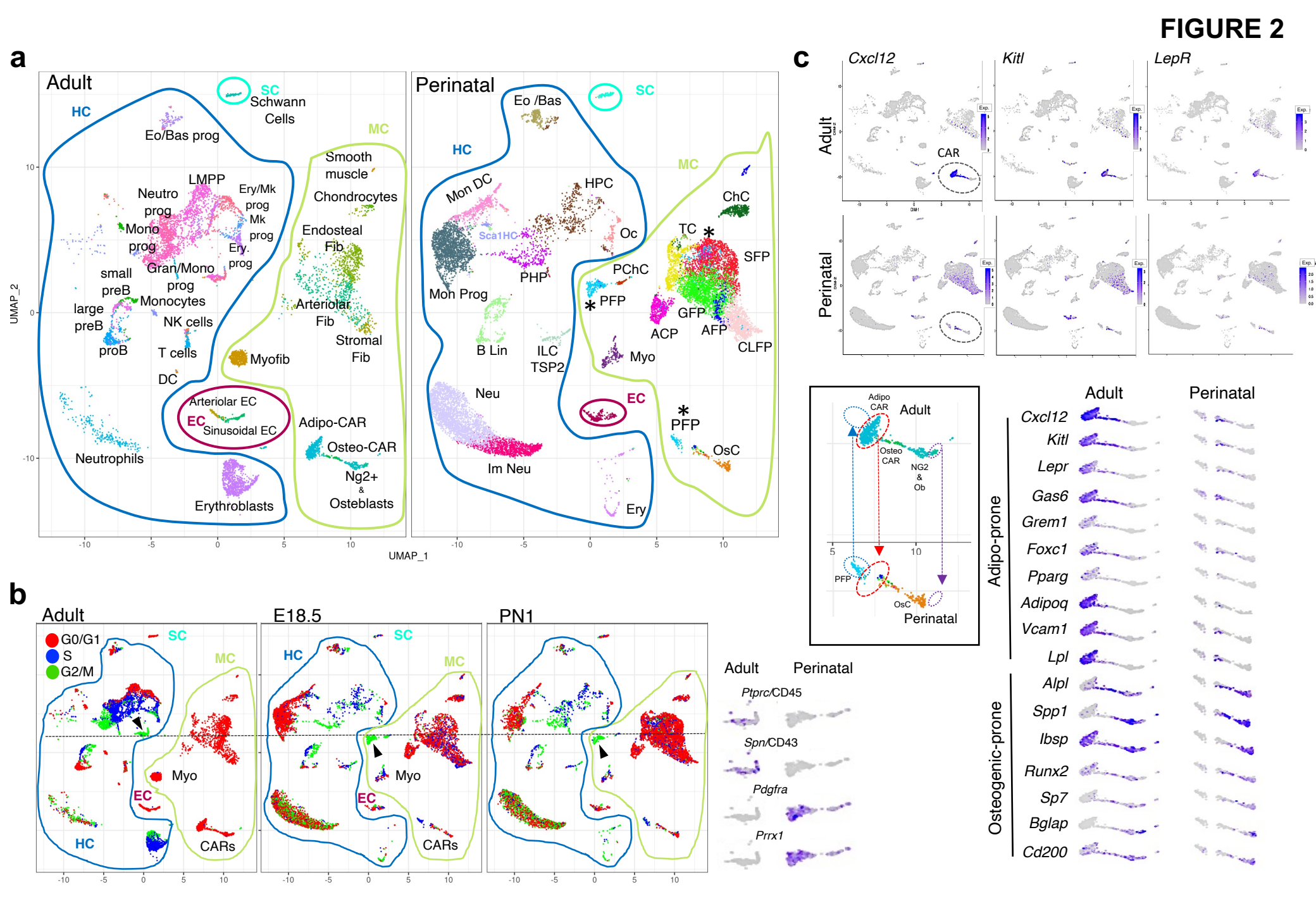
a
Adult
Perinatal
HC
MC
SC
Schwann Cells
Eo/Bas prog
Eo /Bas
LMPP
Neutro prog
Ery/Mk prog
Mk prog
Mono prog
Ery. prog
Gran/Mono prog
small preB
large preB
proB
Monocytes
NK cells
T cells
DC
Neutrophils
Erythroblasts
Arteriolar EC
EC
Sinusoidal EC
Myofib
Smooth muscle
Chondrocytes
Endosteal Fib
Arteriolar Fib
Stromal Fib
Adipo-CAR
Osteo-CAR
Ng2+ & Osteblasts
Mon DC
Sca1HC
Mon Prog
HPC
PHP
Oc
PChC
PFP
B Lin
ILC TSP2
Myo
Neu
Im Neu
Ery
ChC
TC
SFP
GFP
AFP
ACP
CLFP
OsC
UMAP_1
UMAP_2
b
Adult
E18.5
PN1
G0/G1
S
G2/M
Myo
CARs
Ptprc/CD45
Spn/CD43
Pdgfra
Prrx1
c
Cxcl12
Kitl
LepR
CAR
Adipo CAR
Osteo CAR
NG2 & Ob
Adipo-prone
Osteogenic-prone
Lepr
Gas6
Grem1
Foxc1
Pparg
Adipoq
Vcam1
Lpl
Alpl
Spp1
Ibsp
Runx2
Sp7
Bglap
Cd200

FIGURE 3

a

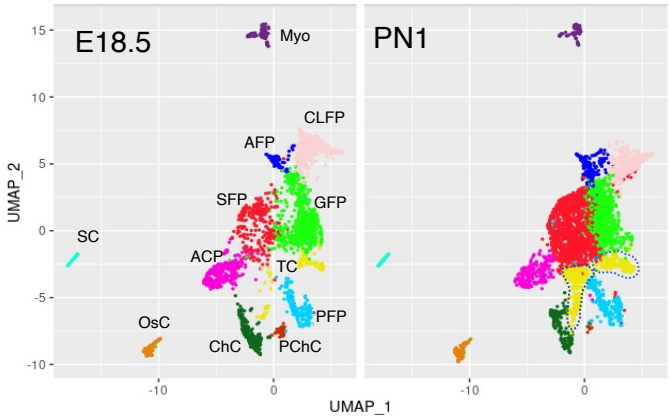

b

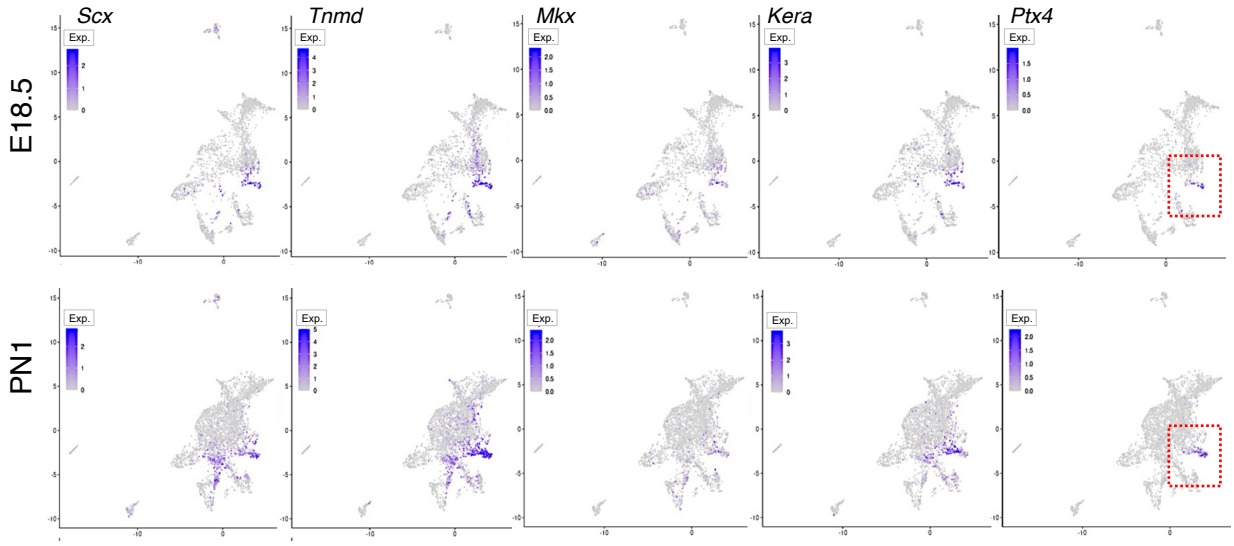

c

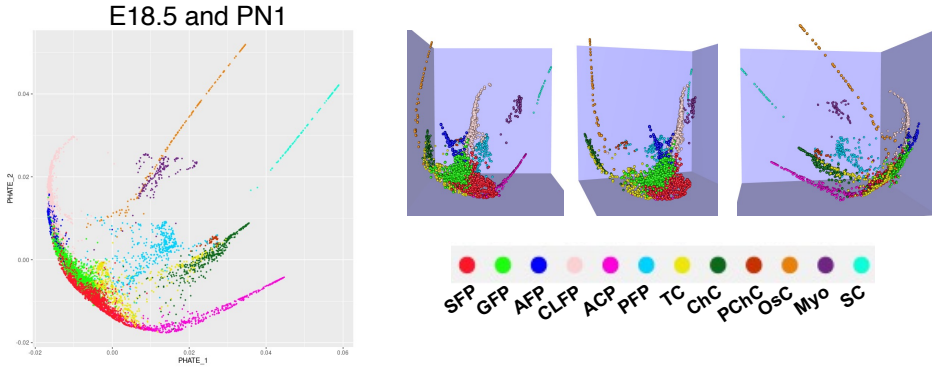

d

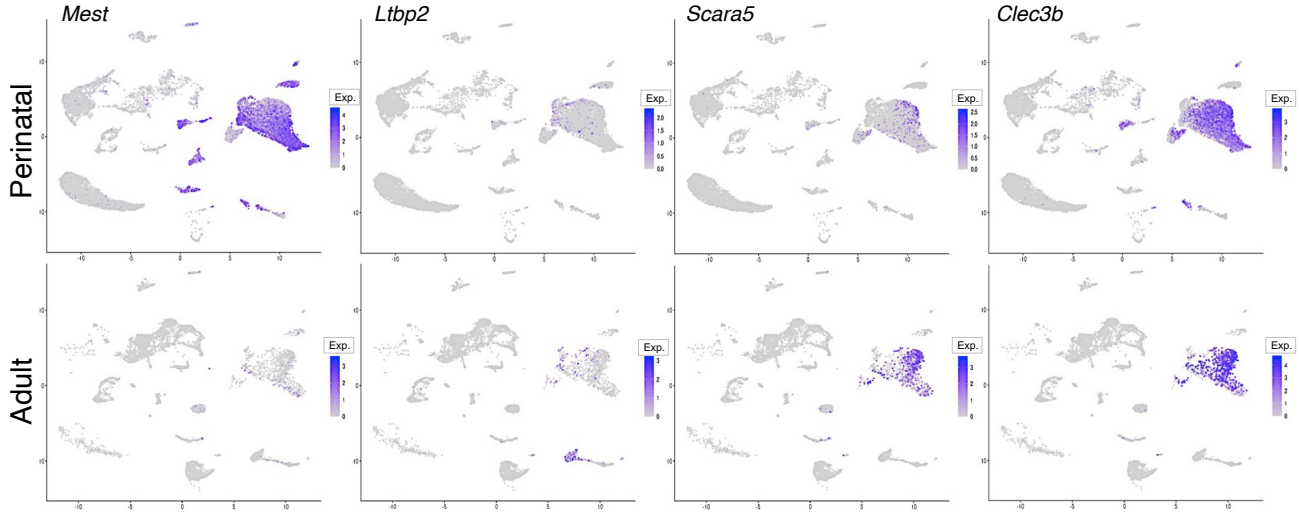

FIGURE 4

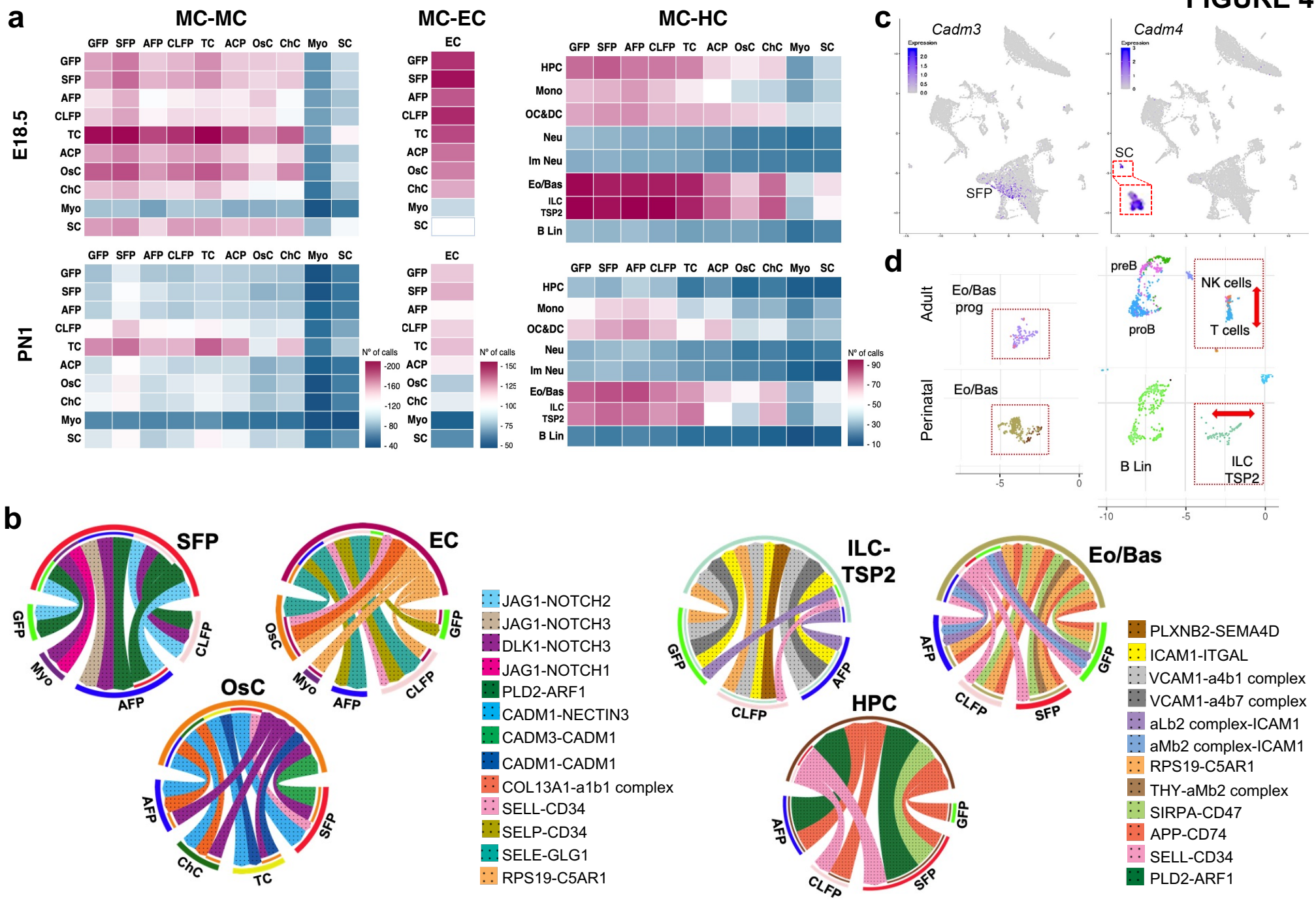
a
MC-MC
MC-EC
MC-HC
E18.5
PN1
GFP SFP AFP CLFP TC ACP OsC ChC Myo SC
EC
HPC
Mono
OC&DC
Neu
Im Neu
Eo/Bas
ILC TSP2
B Lin
Nº of calls
c
Cadm3
Cadm4
SFP
SC
d
Adult
Perinatal
Eo/Bas prog
Eo/Bas
preB
proB
NK cells
T cells
B Lin
ILC TSP2
b
SFP
EC
OsC
ILC-TSP2
Eo/Bas
HPC
JAG1-NOTCH2
JAG1-NOTCH3
DLK1-NOTCH3
JAG1-NOTCH1
PLD2-ARF1
CADM1-NECTIN3
CADM3-CADM1
CADM1-CADM1
COL13A1-a1b1 complex
SELL-CD34
SELP-CD34
SELE-GLG1
RPS19-C5AR1
PLXNB2-SEMA4D
ICAM1-ITGAL
VCAM1-a4b1 complex
VCAM1-a4b7 complex
aLb2 complex-ICAM1
aMb2 complex-ICAM1
RPS19-C5AR1
THY-aMb2 complex
SIRPA-CD47
APP-CD74
SELL-CD34
PLD2-ARF1

FIGURE 5

a

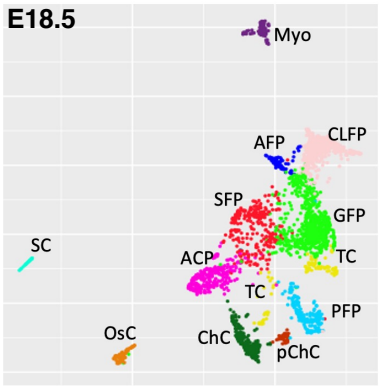

Regulons (+) controlling *genes*

Klf3	*Atf3*	*Nfkb1*	*Cebpd*
Klf3 (+)	**Atf3(+)**	**Nfkb1 (+)**	**Cebpd(+)**
Hoxa7 (+)	**Cebpd (+)**	**Atf3 (+)**	Gata6 (+)
Hoxd9(+)	Gsc (+)	Bcl3 (+)	Irf1 (+)
Lhx9 (+)	Erg1 (+)	Erg3 (+)	
Fosl1 (+)	Fosl1 (+)	Fosl1 (+)	
Foxc1 (+)	Cebpb (+)	Cebpb (+)	Tcf7l2(+)
	Gata6 (+)	Irf8 (+)	Meox1(+)
	Jun (+)	Spi1 (+)	Jun (+)
	Rel (+)	Rel (+)	
	Nfil3 (+)		
	Fosb (+)		
	Maff (+)		

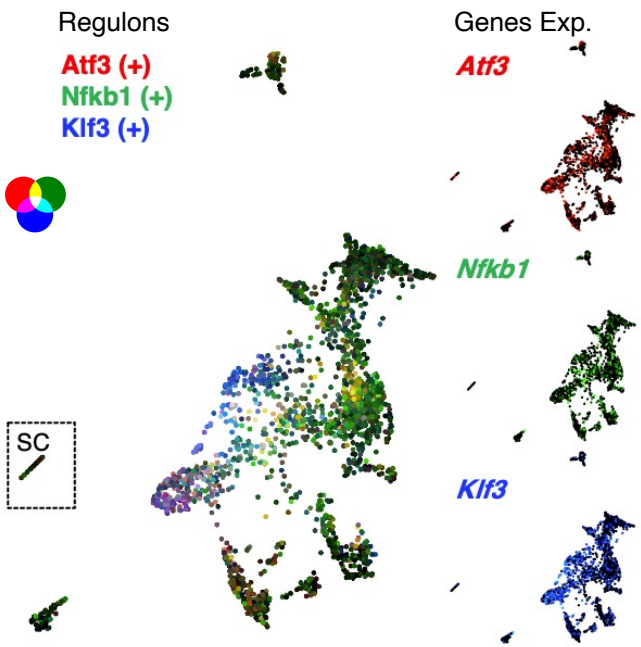

b

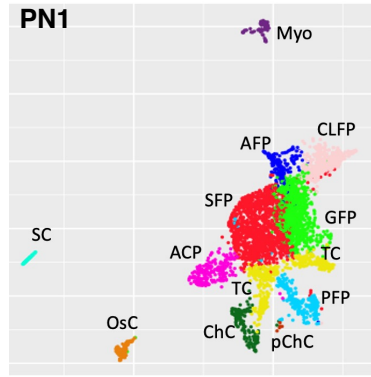

Regulons (+) controlling *genes*

Klf4	*Atf3*	*Nfkb1*	*Cebpd*	*Nr1d1*
Klf4 (+)	**Atf3 (+)**	**Nfkb1 (+)**	**Cebpd(+)**	**Nr1d1 (+)**
Atf3 (+)	**Cebpd (+)**	**Atf3 (+)**		
Barx1 (+)	Barx1 (+)	Bcl3 (+)	Tcf7l2(+)	
Fosb (+)	Fosb (+)	Maff (+)	Irf1(+)	Irf8 (+)
Fosl1 (+)	Fosl1 (+)			Fosl1(+)
Foxc1 (+)	Foxc1 (+)	Spi1 (+)	Spi1(+)	
Foxd1 (+)	Ceppb (+)			
Irx3 (+)	Irx3 (+)			
Jun (+)	Jun (+)		Jun (+)	
Stat2 (+)		Stat2 (+)	Stat2 (+)	
	Nfkb1 (+)			**Nfkb1 (+)**
	Ddit3 (+)			Ppard(+)
	Junb (+)	Junb (+)		

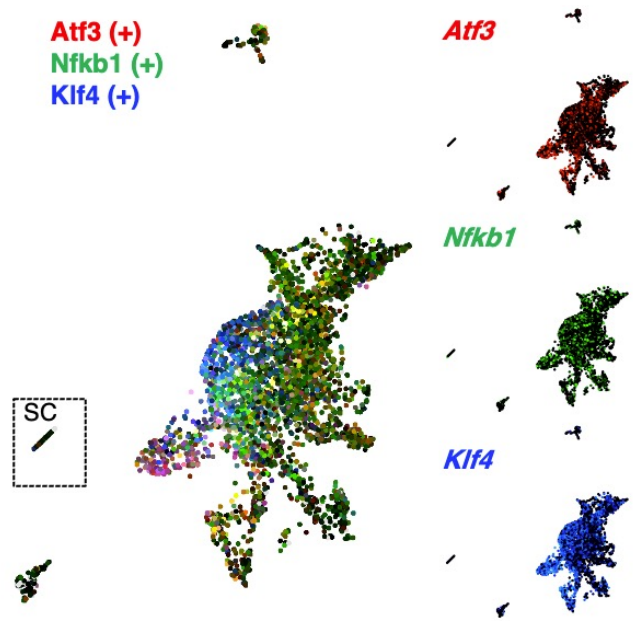

FIGURE 6

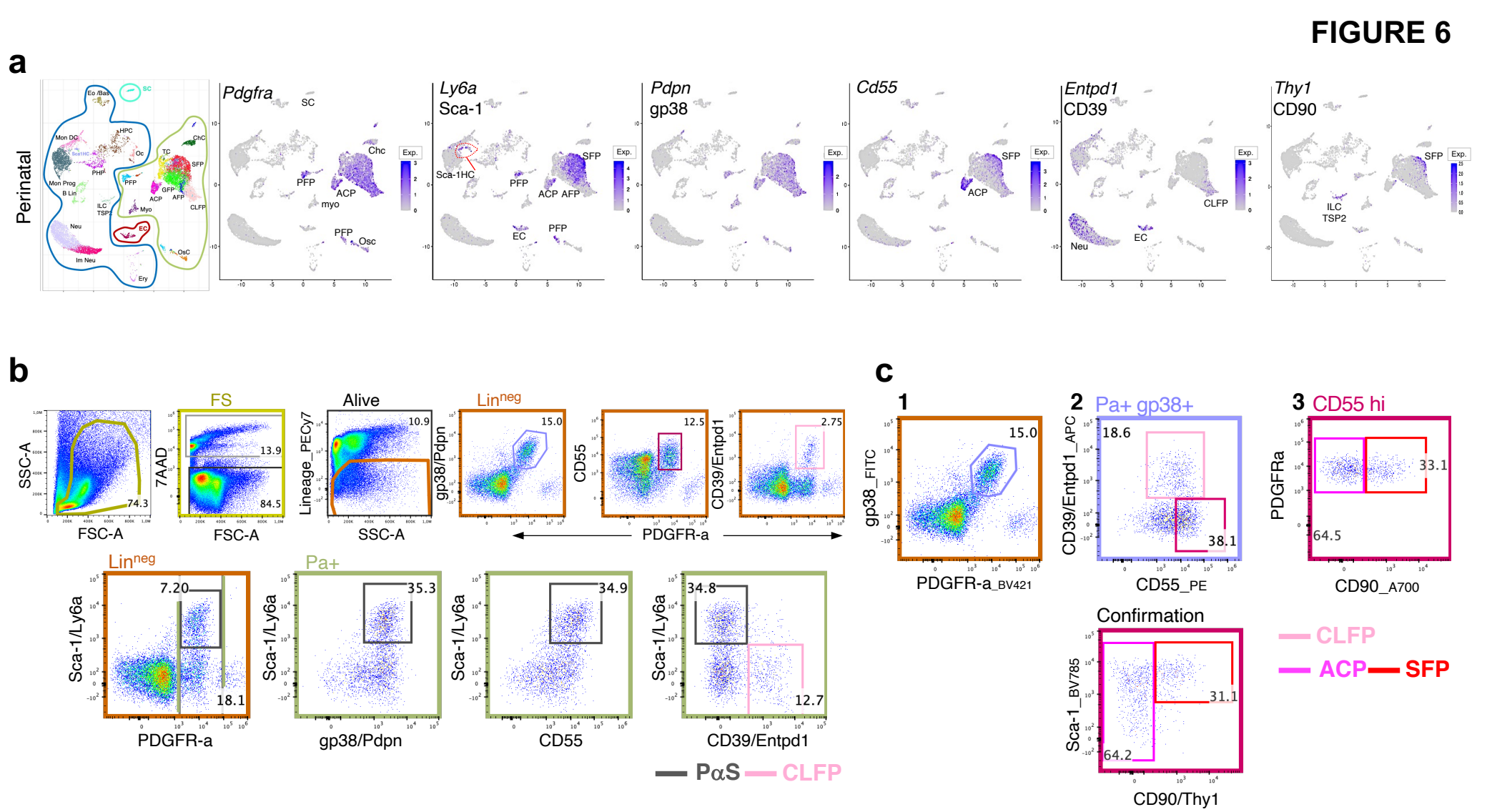
a
Perinatal
Pdgfra
Ly6a
Sca-1
Pdpn
gp38
Cd55
Entpd1
CD39
Thy1
CD90
b
FS
Alive
Lin^neg
Pa+
SSC-A
FSC-A
7AAD
Lineage_PECy7
gp38/Pdpn
CD55
CD39/Entpd1
PDGFR-a
Sca-1/Ly6a
PαS
CLFP
c
1
2 Pa+ gp38+
3 CD55 hi
gp38_FITC
PDGFR-a_BV421
CD39/Entpd1_APC
CD55_PE
PDGFRa
CD90_A700
Confirmation
Sca-1_BV785
CD90/Thy1
CLFP
ACP
SFP